ORIGINAL RESEARCH

Toxicity and Oxidative Stress Biomarkers in the Organs of Mice Treated with Mesoporous Polydopamine Nanoparticles Modified with Iron and Coated with Cancer Cell Membrane

Marta Szukalska [ID][1], Bartosz F Grześkowiak[2], Magdalena J Bigaj-Józefowska[2], Marta Witkowska [ID][3,4], Emilia Cicha[5], Patrycja Sujka-Kordowska[6], Izabela Miechowicz [ID][7], Michał Nowicki[6], Radosław Mrówczyński [ID][3,4], Ewa Florek [ID][1]

[1]Laboratory of Environmental Research, Department of Toxicology, Poznan University of Medical Sciences, Poznań, Poland; [2]NanoBioMedical Centre, Adam Mickiewicz University, Poznań, Poland; [3]Faculty of Chemistry, Adam Mickiewicz University, Poznań, Poland; [4]Centre for Advanced Technologies, Adam Mickiewicz University, Poznań, Poland; [5]Laboratory of Experimental Animals, Poznan University of Medical Sciences, Poznań, Poland; [6]Department of Histology and Embryology, Poznan University of Medical Sciences, Poznań, Poland; [7]Department of Computer Science and Statistics, Poznan University of Medical Sciences, Poznań, Poland

Correspondence: Marta Szukalska, Laboratory of Environmental Research, Department of Toxicology, Poznan University of Medical Sciences, Rokietnicka 3 Street, Poznan, 60-806, Poland, Email martan@ump.edu.pl

Purpose: Polydopamine nanoparticles (PDA NPs) have great potential in medicine. Their applications being widely investigated in cancer therapy, imaging, chemotherapy, photodynamic therapy (PDT), photothermal therapy (PTT), and tissue repair. The aim of our study was to assess the in vivo toxicity and changes in oxidative stress biomarkers in organs of animals treated with mesoporous PDA NPs modified with iron (MPDAFe NPs), coated with the cancer cell membrane and loaded with doxorubicin (DOX), and subsequently subjected to PTT.

Methods: Liver and kidney homogenates were obtained from BALB/c nude mice with xenograft HepG2 human hepatoma cells, treated with iron modified mesoporous PDA nanoparticles, coated with the cancer cell membrane and loaded with doxorubicin (MPDAFe@DOX@Mem NPs), and subjected to PTT. These samples were used for histological evaluation and measurement of oxidative stress biomarkers, including total protein (TP), reduced glutathione (GSH), nitric oxide (NO), S-nitrosothiols (RSNO), thiobarbituric acid reactive substances (TBARS), trolox equivalent antioxidant capacity (TEAC), catalase (CAT), glutathione S-transferase (GST), and superoxide dismutase (SOD).

Results: In the kidney, MPDAFe@DOX@Mem NPs in combination with PTT increased GSH (43%), TBARS (32%), and CAT (27%), while SOD decreased by 20% compared to the control group. Additionally, CAT activity in the liver increased by 79%.

Conclusion: Significant differences in oxidative stress parameters and histological changes after administration with MPDAFe@DOX@Mem NPs and PTT were observed in the kidneys, showing more pronounced changes than the liver, indicating potential kidney toxicity. Our research provides insights into oxidative stress and possible toxic effects after in vivo administration of mesoporous PDA NPs combined with chemotherapy-photothermal therapy (CT-PTT), which is extremely important for their future applications in anticancer therapies.

Keywords: polydopamine nanoparticles, oxidative stress, liver cancer model, in vivo toxicity, chemo- and photothermal therapy

Introduction

Polydopamine is a biopolymer obtained by polymerization of dopamine monomers, inspired by compounds used by mussels to stick to various surfaces.[1,2] Polydopamine nanoparticles have been of great interest to researchers for over fifteen years and have found a wide application in many areas of material chemistry, tissue engineering, implants, and nanomedicine.[3–7] The successful use of this biomimetic polymer to create various materials applied in medicine can be attributed to a set of unique

Graphical Abstract
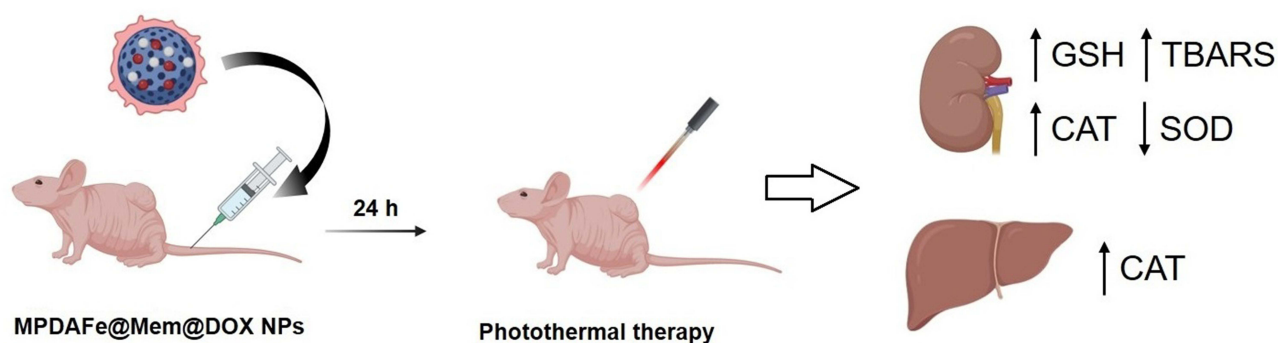
physicochemical properties. The good adhesive properties of PDA allow it to cover virtually any type of material, including hydrophobic surfaces and various groups of nanoparticles and scaffolds. It is worth emphasizing that PDA is known to chelate almost all kinds of metals. This enables the attachment of paramagnetic metal ions to nanomaterials, providing them with contrast properties for MRI, which is particularly valuable for diagnostic approach.[6,8] Additionally, a wide range of PDA functionalization methods have been described for biomolecules and polymers for various applications.[6,7,9–11]

The first major turning point for the role of polydopamine in nanomedicine was its use as a nanocarrier for drug delivery.[12] Thanks to its catechol, amine, and quinone groups, PDA can react with drugs by enabling the anchoring of functional molecules.[6,7] Besides, PDA easily reacts with bioactive compounds that contain thiol or amine groups through Michael addition or Schiff base reactions.[13] The result of these modifications is the granting completely new functions to nanoparticles, such as targeting, imaging, chemical treatment, photodynamic therapy, photothermal therapy, and tissue repair.[6,14] Therefore, polydopamine nanomaterials are a promising candidates for the development of novel cancer treatment strategies.[15–18] Polydopamine has an outstanding drug-loading capability and a high potential for targeted drug delivery.[17,19] It was demonstrated that PDA possesses strong photothermal properties.[20–22]

Furthermore, many studies indicate that it can be used for cancer diagnostic purposes.[3,17,21] Polydopamine-modified nanomaterials can serve as platforms for carrying anticancer drugs and radionuclides in one system, while enabling radionuclide imaging of the tumor and inhibiting tumor development and proliferation.[23] Due to the fact that PDA nanoparticles are marked by high biocompatibility, easy and cost-effective production, and can emit fluorescence when excited with ultraviolet (UV) or visible light, they can be used as tumor imaging agents.[16]

Polydopamine nanoparticles, however, face challenges such as instability in circulation and inadequate tissue targeting. In recent years, biological membranes have been intensively researched as ideal candidates for improving the biosafety and targeting properties of polymeric nanoparticles.[24] Membranes of living cells, such as erythrocytes, white blood cells, or cancer cells, can be isolated and coated around the nanocarriers. Cancer cell membrane coatings have been proven to increase the efficacy of anticancer treatment of iron modified mesoporous PDA nanoparticles loaded with drug (MPDAFe@DOX@Mem NPs) by enhancing internalization and targeting to hepatocellular carcinoma cells.[25]

One of polydopamine's most important role is its potential participation in antioxidant protection.[26] Polydopamine helps protect cells in diseased or inflammatory states from oxidative stress and shows activity against various ROS-related diseases.[27,28] Oxidative stress is a state of cells and tissues in the body that is known by an imbalance between the production of reactive oxygen species (ROS) and the ability to neutralize these factors and the damage they cause. Some studies confirmed that PDA can scavenge superoxide anions and hydroxyl radicals.[29] PDA's antioxidant properties are considered to be related to the presence of catechol groups in the molecule, which can provide hydrogen atoms from phenolic hydroxyl groups to quench free radicals.[20,26] On the other hand, it can reduce some compounds by electron transfer. The phenoxy radical thus formed reacts with the second radical, creating stable quinone structures.[30] Moreover, PDA nanomaterials reduce the amount of pro-inflammatory cytokines (IL-1β, IL-6 and TNF-α) and the inflammatory

mediator COX-2.[29,30] The antioxidant mechanism of polydopamine can be also related to other PDA's features; such as: dissipation of radiant energy to inhibit the formation of free radicals, detoxification of reactive oxygen species, and regulation of the activity of the body's defense factors.[30] Although PDA materials have been reported to eliminate ROS both in vitro and in vivo, their potential antioxidant performance in cancer treatment has not yet been well explored.

Our study aimed to evaluate the in vivo toxicity of MPDAFe@DOX@Mem NPs through histological evaluation of tissues and assessment of oxidative stress biomarkers, including: total protein (TP), reduced glutathione (GSH), nitric oxide (NO), S-nitrosothiols (RSNO), thiobarbituric acid reactive substances (TBARS), trolox equivalent antioxidant capacity (TEAC), catalase (CAT), glutathione S-transferase (GST), and superoxide dismutase (SOD) in liver and kidney homogenates obtained from a HepG2-xenograft nude mouse model subjected to combined chemo- and photothermal therapy. An understanding of the influence of PDA NPs' presence on the mechanism of oxidative stress and its role in cancer and combined CT-PTT may improve the therapeutic outcomes of existing, and influence the design of new therapies to treat liver cancer. Therefore, the presented data are significant in the matter of the PDA nanomaterials and their translation potential in future anticancer treatment.

Materials and Methods
Nanomaterials Synthesis and Characterization
Cell Membrane Coated MPDAFe Nanoparticle Synthesis
The porous PDAFe nanoparticles were synthesized using a previously established protocol for Fe-modified mesoporous PDA nanoparticles.[25] Briefly, 0.36 g of Pluronic® F-127 was dissolved in 60 mL ethanol and 65 mL water. Then, 0.36 g of 1,3,5-trimethylbenzene (TMB) was added and mixed for 30 min, followed by the addition of 90 mg of Trizma base in 10 mL of water and 60 mg of dopamine hydrochloride, and left under stirring for 24 h. 360 mg of iron(III) chloride hexahydrate was added 5 h prior to the termination of the synthesis. The nanoparticles were washed with a mixture of ethanol and acetone (2:1 v/v%) and 30 min sonication followed by high-speed centrifugation.

The nanoparticles were loaded with doxorubicin by mixing MPDAFe NPs (1 mg/mL in 7.4 pH PBS buffer) with DOX solution (1 mg/mL in pH 7.4 PBS buffer) in 2:1 volume ratio. The mixture was kept under shaking overnight and then purified by several cycles of washing with pH 7.4 PBS buffer (until a clear supernatant was obtained after centrifugation).

Human hepatocellular carcinoma HepG2 cells, commercially purchased (ATCC® Number: HB-8065™, Lot Number: 63176294), were used as the source of cancer cell membranes. The membranes containing natural membrane proteins were isolated using Mem-PER™ Plus Membrane Protein Extraction Kit. The membrane vesicles were obtained by extruding the membrane solution 20 times through a polycarbonate membrane (pore size 0.8 μm) using an Avanti® mini extruder (Avanti Polar Lipids, USA) device equipped with gas-tight syringes.

MPDAFe or MPDAFe@DOX nanoparticles (1 mg/mL in water) were mixed with the solution of the membrane vesicles (1 mg of protein per 1 mL of water). The mixture was then sonicated with a high-energy sonicator (500 W, A = 25%, pulse mode – 1 s on, 2 s off, total time 1 min 30s). Then, the solution was extruded 10 times through a polycarbonate membrane (pore size 0.8 μm).

Nanoparticles Characterization
The hydrodynamic diameter and zeta potential of NPs were measured using the Zetasizer Nano ZS apparatus (Malvern Panalytical, UK).

The TEM images were obtained using the Transmission Electron Microscope JEM-1400 (JEOL, Japan) by drop casting a diluted sample on a Lacey Formvar/Carbon grid (300 mesh, Copper approx. grid hole size: 63 μm) and left to dry overnight. To visualize the membrane coating of the coated nanoparticles, a drop of 1% uranyl acetate was added to the grid containing the nanoparticles and left to dry overnight.

The iron content was evaluated using ICPOES VISTA-MPX (Varian, USA) by dissolving 1 mg of dry MPDAFe NPs in nitric acid overnight at 50°C.

The DOX loading and release were established by UV–Vis measurements (UV/Vis/NIR Spectrophotometer LAMBDA 950 (Perkin Elmer, USA)).

The photothermal effect was evaluated using two complementary methods. A 1 mL of sample of 100 µg/mL concentration was irradiated for 5 min with an 808 nm laser (Changchun New Industries Optoelectronics Tech. Co. Ltd., China) with a power density of 6 W/cm². The temperature changes were registered either with a thermocouple (with 10s intervals) or thermal imaging camera (SONEL KT-650, Poland) (images taken every 1 min). The temperature changes of 1 mL of water were registered as a control.

Experimental Model

Ethics Committee Approval

The Local Ethics Committee for Animal Experiments in Poznan, Poland, authorized the study design (Approval No. 5/2020 of 13.03.2020; 6/2022 of 25.02.2022). All laboratory animal handling and usage methods followed European Union (UE) laws under Directive 2010/63/EU on animal protection for research purposes. To safeguard animals, experiments were conducted by the "3Rs" principle (Replacement, Reduction, and Refinement). To ensure consistent results, the study focused on the minimum number of animals and observation time. To improve the rigor and reproducibility of animal research, all data were collected using the ARRIVE 2.0 guidelines. Experiments were carried out in the Laboratory of Experimental Animals at Poznan University of Medical Sciences in Poland. The Laboratory of Experimental Animals is a unit listed by the Ministry of Science and Higher Education. Contractors have individual permits for planning and performing experiments.

Animals

The experiment involved 56 female BALB/c nude mice with Health certificate CRL with the following characteristics: CAnN.Cg-Foxn1nu/Crl, an outbred herd at 5 weeks old, with an average body weight of 17.20 ± 1.20 g (Charles River Laboratories, Germany). To ensure trustworthy results and minimize the number of used animals, only female animals were employed in the experiment. Mice were kept in GM500 polypropylene cages (Tecniplast, Buguggiate, Italy) with autoclaved aspen bedding ($2 \times 2 \times 1$ mm) under regulated environmental conditions (12 h light/12 h dark: 6 am-6 pm; temperature: $22 \pm 2°C$; air humidity: 50–60%). To improve the animals' living conditions, materials for building sockets, shelters, and teeth grinding blocks (Tapvei, Estonia) were placed in their cages. The animals were acclimated to laboratory conditions (Experimental Animal Laboratory) two weeks before the trial began. They had free access to water and a nutritious diet. The animals were fed using the 1414 Forti formula (Altromin, Lage, Germany). We followed the Ethics Committee for Animal Experiments Affairs in Poznań, Poland when conducting animal studies to ensure ethical compliance. After two weeks of acclimatization, female BALB/c (CAnN.Cg-Foxn1nu/Crl) nude mice (groups I–VIII) were subcutaneously injected with 2×10^6 HepG2 cells in 100 µL PBS. When tumor volumes reached 80 mm³, the animals were used for further investigation. Tumor volume was determined by multiplying tumor length by tumor breadth and dividing by two.

Experimental Design

Mice with induced tumors were divided into 8 groups (I–VIII), each of 7 individuals. Group I animals were administrated with a single dose of 100 µL of a phosphate-buffered saline solution (PBS) into the tail vein. Group II animals were administered with a single dose of 4.44 mg/kg body weight (bw) in 100 µL PBS buffer solution (vehiculum) with mesoporous PDA nanoparticles modified with iron coated with the cancer cell membrane (MPDAFe@Mem) with prolonged blood circulation time, and active targeting of cancer cells in a mice model of liver cancer.

Mice from group III received a single dose of the anticancer drug, doxorubicin (2 mg/kg bw) in 100 uL of PBS solution into the tail vein. Mice from group IV received 100 µL of doxorubicin-loaded nanoparticles solution MPDAFe@DOX@Mem. Group V mice were once administered 100 µL of PBS into the tail vein, and after 24 h the tumor was irradiated with a laser with a wavelength of $\lambda = 808$ nm (6 W/cm²) for 5 minutes. Mice from group VI received a single dose of MPDAFe@Mem (4.44 mg/kg bw), and were subjected to laser irradiation after 24 h. Group VII animals received 100 µL of DOX solution (2 mg/kg bw) and were laser-irradiated after 24 h. Mice from group VIII received a single dose of MPDAFe@DOX@Mem into the tail vein and after 24 h were irradiated with a laser. The representation of the experimental design is shown in Figure 1.
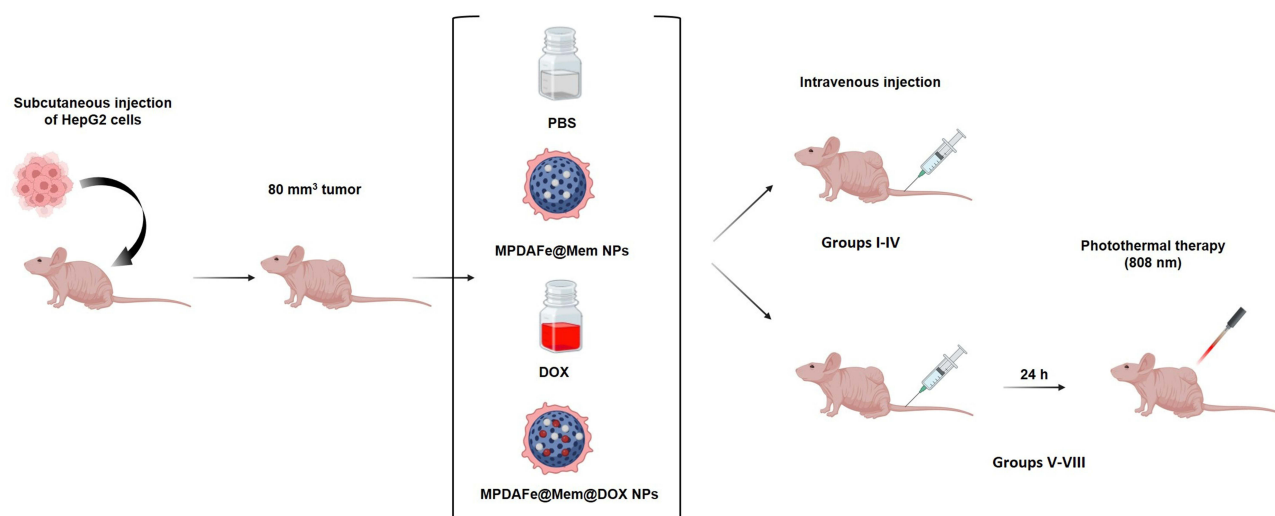
12056

DovePress

International Journal of Nanomedicine 2024:19

Figure I Schematic representation of the experimental design. Created with BioRender.

After completing the observation, the animals had been subjected to an autopsy. Solution of ketamine (90 mg/kg; Kepro, Woerden, The Netherlands) and xylazine (10 mg/kg; Kela, Hoogstraten, Belgium) was intramuscularly administered to mice for anesthesia. Following the introduction of deep anesthesia, the animals were sacrificed by taking blood from the heart, and the organs and tumors were harvested and weighed (Laboratory scale, AXIS AC220 [220g/0001g]). Liver and kidney samples were divided and appropriately preserved for further histological and biochemical analyses.

Histological Examination of Liver and Kidney Tissues

The samples of mouse kidneys and liver tissue from all of the analyzed groups were collected for histological examination.

Immediately after collection, the tissues were placed in a 10% formalin solution and fixed for at least 48 h. Subsequently, the samples were washed in water for 24 h, then dehydrated in increasing concentrations of ethyl alcohol (50%, 70%, 85%, 96%, absolute alcohol) and xylene, and embedded in paraffin blocks. The sections of 3–4 μm thickness were prepared from the collected tissue fragments using a semi-automatic rotary microtome (Leica RM 2145, Leica Microsystems, Nussloch, Germany). The sections were then subjected to conventional hematoxylin and eosin (H&E) staining. The samples were deparaffinized, rehydrated, stained with H&E, dehydrated again, and then mounted in a mounting medium on glass slides. The histological preparations were examined using a light microscope, and selected images were captured using a high-resolution and 40x magnification scanner Grundium Ocus®40 (Grundium, Tampere, Finland).

Preparation of Tissue Homogenates

Biochemical analyses were performed at the Environmental Research Laboratory of the Department of Toxicology, Poznań University of Medical Sciences based on previously established protocols.[26,31] Liver or kidney samples were cut into small pieces. A 0.25 g of the tissue was weighed and 2 mL of PBS buffer (Sigma-Aldrich, St. Louis, MO, USA) was added. Tissues were homogenized at 24,000 rpm, then centrifuged (Eppendorf Centrifuge 5804 R) for 10 minutes at 4200 rpm at 4°C. The supernatant was transferred to 2 mL Eppendorf tubes and centrifuged for another 10 minutes at 6000 rpm at 4°C. The resulting supernatant was divided and frozen at −80°C until appropriate determinations.

Determination of Oxidative Stress Biomarkers

Well-known markers of oxidative stress and biochemical parameters (TP, TEAC, RSNO, NO, TBARS, GSH, GST, SOD, CAT) were determined in tissue homogenates using spectrophotometric methods (Spectrophotometer UV-VIS 160, Shimadzu). All chemicals used for biochemical determinations were of analytical reagent grade (Sigma Aldrich).

Total protein (TP) concentration was measured using Lowry's method, a combination of a biuret test and Folin-Ciocalteu reaction.[32]

The trolox equivalent antioxidant capacity (TEAC) of substances present in the solutions was assessed based on the measurement of stable radical cation reduction capacity (ABTS)•+.[33] The concentration of S-nitrosothiols (RSNO) was measured using the Saville/Gries method.[34,35] The concentration of stable degradation products, nitrates(V) and nitrates (III) (nitrites) in an aqueous solution were used to determine NO concentrations.[36] Thiobarbituric acid reactive substances (TBARS) measurement was used for monitoring lipid peroxidation.[37]

Quantitative determination of reduced glutathione (GSH) was performed using modified Ellman's method with 5.5′-dithiobis(2-nitrobenzoic acid) (DTNB, Ellman's reagent).[38] Glutathione S-transferase (GST) enzymatic activity was assessed based on the coupling reaction of thiol groups of L-glutathione with 1-chloro-2,4-dinitrobenzene (CDBN).[39]

The activity of superoxide dismutase (SOD) was estimated by a method based on the capacity to inhibit adrenaline autoxidation by SOD. The assumed enzyme activity in the evaluated sample was the enzyme amount that causes 50% inhibition of adrenaline autoxidation to adrenochrome ($\Delta A/min = 0.025$) in the same analytic conditions.[39]

The activity of catalase (CAT) was determined based on the reaction of H_2O_2 degradation. The unit of CAT activity is the enzyme amount that degrades 1 μM H_2O_2 solution within 1 minute, which corresponds to absorbance reduction by 0.036 U/min (volume: 1 mL, optical path length: 1 cm).[39]

Statistical Analysis

Calculations were performed using Statistica 13 by Tibco and PQStat by PQStat Software. The level of significance was $\alpha=0.05$. The result was considered statistically significant when $p<\alpha$. The normality of the distribution of variables was tested using the Shapiro–Wilk test. In order to compare variables between 8 groups, in the case of compliance with the normal distribution and equal variances, the analysis of variance test for unrelated samples was performed, and in the case of non-equal variances, the Welch F-test was conducted. Additionally, Fisher's multiple comparisons LSD test was performed. In case of non-compliance with the normal distribution, the Kruskal–Wallis test with the Dunn-Bonferroni multiple comparison test were applied. In order to compare variables between the 2 groups, the Student's t-test was performed for unrelated samples when the distribution was consistent with the normal distribution and the variances were equal, the Cochran-Cox test when the variances were not equal, or the Mann–Whitney test when the distribution was not consistent with the normal distribution.

Results
Characteristics of NPs Used for Treating Mice

The results regarding characterization of MPDAFe NPs are presented in Supporting information. A TEM image shows the spherical morphology of nanoparticle with mesoporous structure (Figure S1). Moreover, darker iron clusters on the surface are visible. The hydrodynamic diameter of MPDAFe NPs was about 250 nm (Table S1), and the zeta potential value was negative (−23 mV) (Table S1). A successful coating was proven by increasing hydrodynamic diameter of about 10 nm, which is in line with the theoretical width of the cellular membrane. The membrane layer around the nanoparticles is visible on uranyl acid stained TEM images (Figure S2). Furthermore, the zeta potential value decreased after the coating and corresponded to the value of membrane vesicles. The DOX loading into MPDAFe NPs was nearly 90%, while the encapsulation efficiency was about 46%. The drug release from MPDAFe@DOX was evaluated in normal (7.4) and acidic (4.5) pH over 124 h (Figure S3). The release of DOX was highly effective at pH 4.5, which resembles the chemical environment of cancer cells. On the contrary, the release of drug was lower at pH 7.4, corresponding to healthy cells. The MPDAFe NPs were suspended in water at a concentration of 100 $\mu g/mL$, and a laser with a power density of 6 W/cm^2 was applied. A significant temperature increase was observed for the NPs, indicating high photothermal conversion effect (Figure S4A). To further visualize the temperature rise for the MPDAFe, photothermal images were captured (Figure S4B). The images exhibited distinct regions of increased temperature, indicating successful heat generation by the NPs upon laser irradiation.

Body Weight and Clinical Signs During the Experiment

Figure 2 shows the body weight variations of the female BALB/c nude mice from the control group (I) and after receiving different treatment methods (group II–VIII). It can be seen that the treatment did not cause a significant body
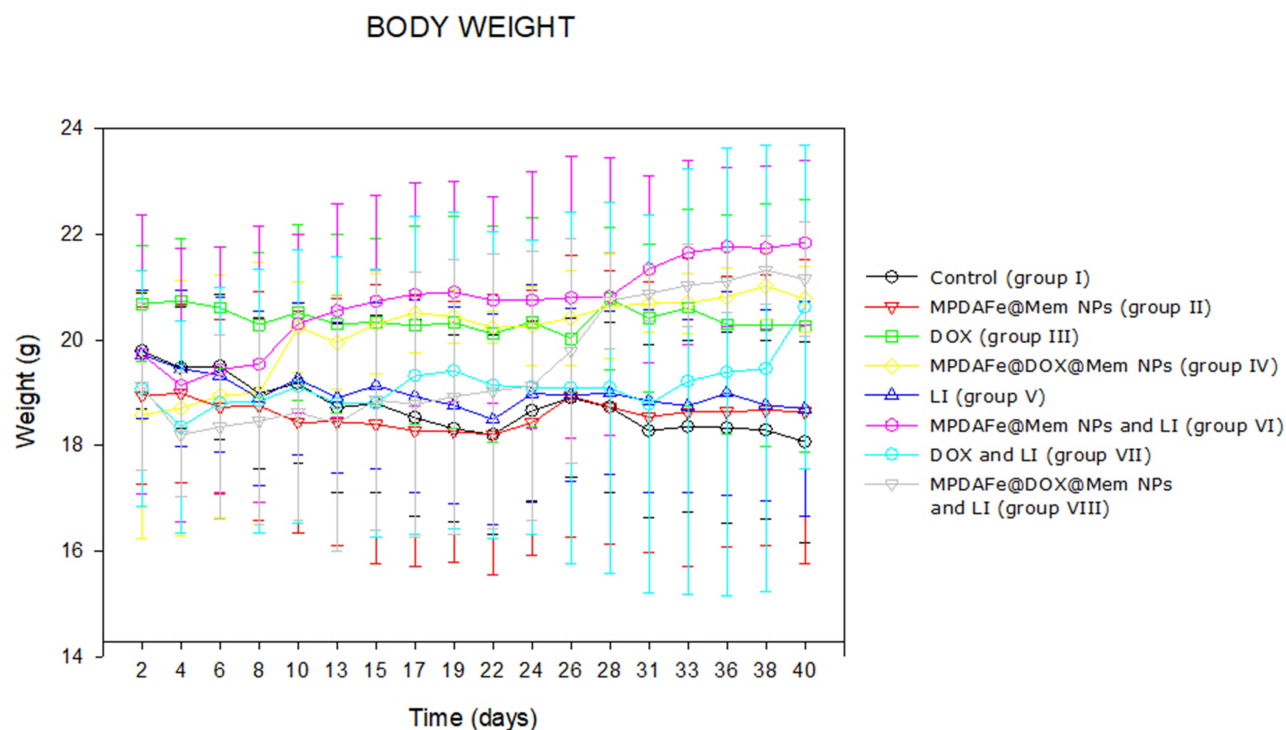
BODY WEIGHT

Figure 2 Mean body weight over time after receiving different treatment methods (group I–VIII).

weight change. A clear decrease in body weight >5% was recorded only for the control group with induced cancer, not subjected to any therapy. Moreover, in the group administered with MPDAFe@Mem NPs in combination with doxorubicin or laser irradiation or both, body weight has a growing tendency in comparison to the control group and groups with other ways of the treatment (groups IV, VI and VIII). The clinical symptoms were stable throughout the whole treatment period.

Final Body and Organ Weights

The average final body weight in the group that received intravenously MPDAFe@Mem NPs without the drug and was subjected to laser irradiation after 24 hours (group VI) was statistically significantly higher than in the control group I, group II, group IV, and group VII (Figure 3A).

We did not note any differences in organ weights (liver, right kidney, left kidney, heart, brain, lungs, pancreas, spleen) between the study groups (Figure 3B–I).

Tumor Size and Weights

Forty days after treatment, tumors were harvested and weighted. We did not observe a statistically significant differences in the average tumor weight between the study groups (Figure 4A and B).

Histological Assessment
Control Group

The liver exhibited a normal architecture. Anatomical lobules with central veins were present. Portal areas with bile ducts and blood vessels were visible. Hepatocytes demonstrated a normal structure. Sinusoids were of normal size (Figure 5A).

The kidneys displayed a normal structure, with the cortex and medulla visible under microscopic examination. In the cortex, renal glomeruli as well as proximal and distal renal tubules were present. Renal corpuscles showed a normal structure, with proper-sized urinary space. Proximal tubules were lined with low cuboidal to columnar epithelium, with narrow lumens. Distal tubules, in fewer numbers, are lined with lower epithelium and have wider lumens (Figure 6A).

Laser Irradiation Group

Discrete features of cytoplasmic degeneration/vacuolization of hepatocytes were visible in the liver, especially in the central part of classic lobules. Locally, microvascularization was intensified (Figure 5B and C).
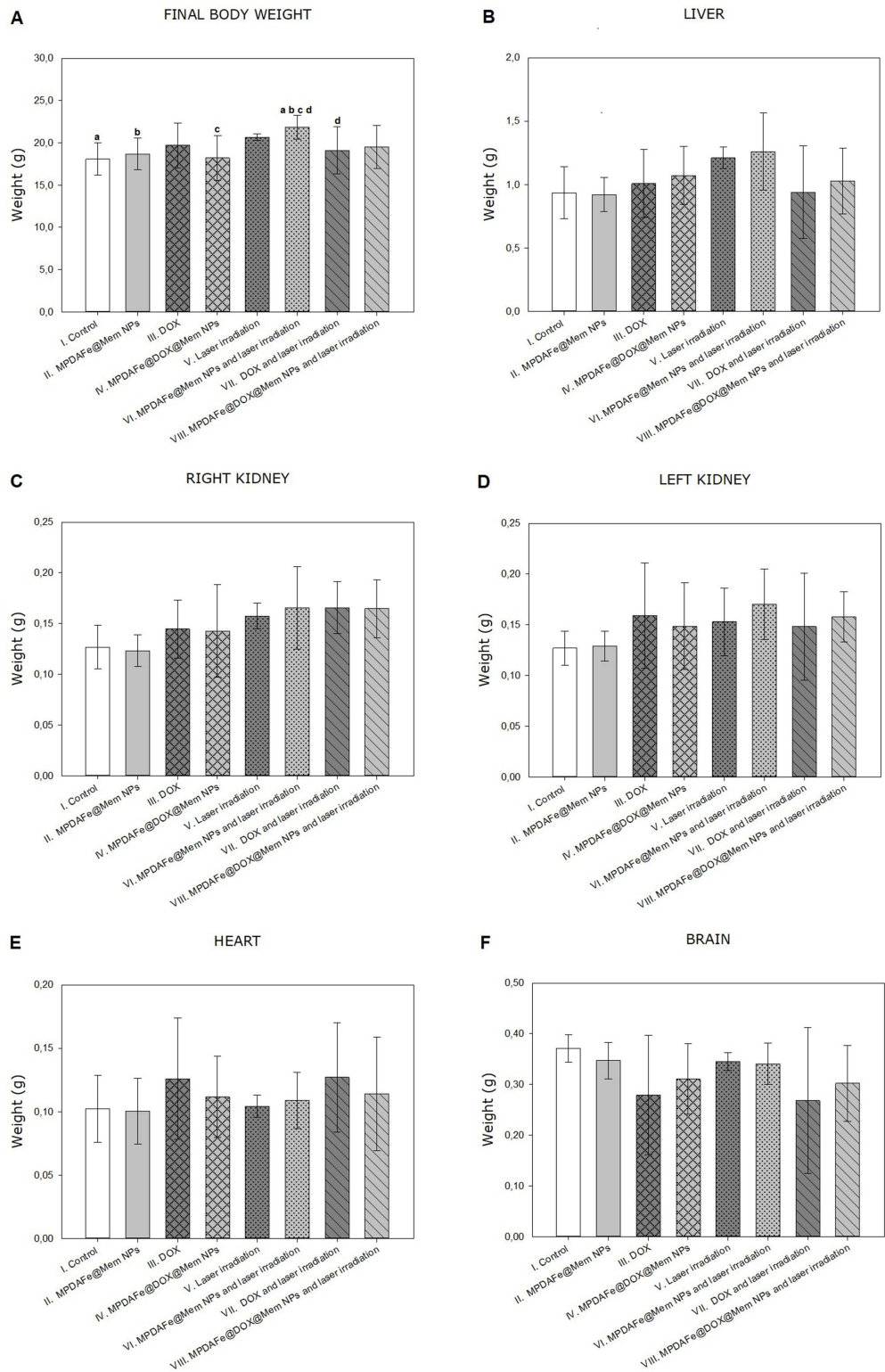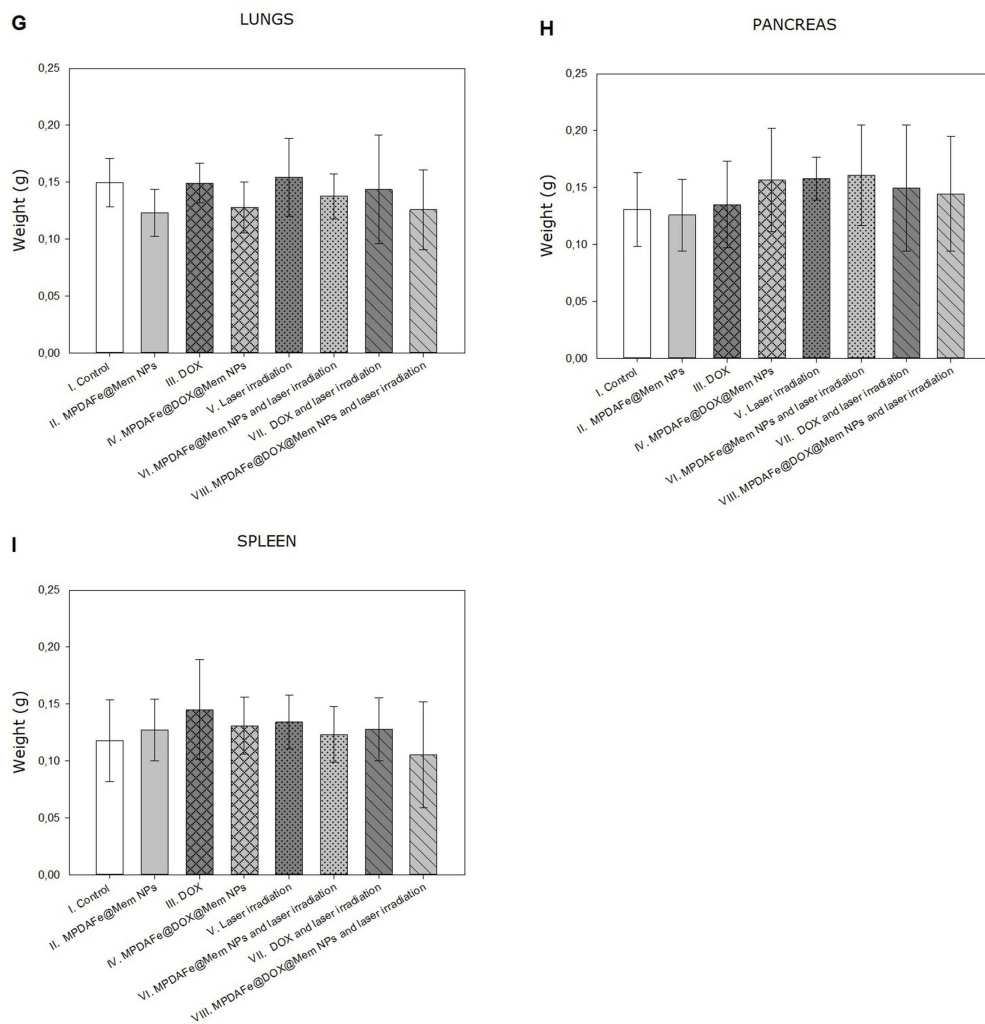

Figure 3 Continued.

Figure 3 Comparison of final body (**A**) and organ weights (**B–I**). Each bar represents mean ± SD value of body and organs (liver, right kidney, left kidney, heart, brain, lungs, pancreas, spleen) weights of BALB/c nude mice on the last day of the experiment. Statistically significant results: a - groups significantly different at p = 0.0044; b - groups significantly different at p = 0.0203; c - groups significantly different at p = 0.0061; d - groups significantly different at p = 0.0350.
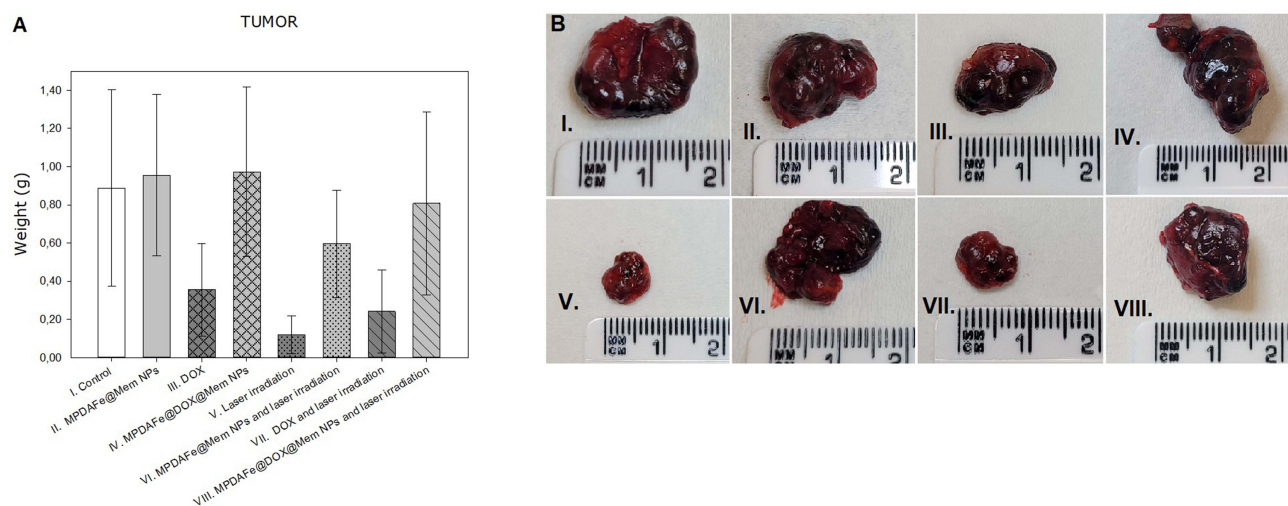

Figure 4 (**A**) Comparison of tumor weights. (**B**) Example pictures of tumor tissues.
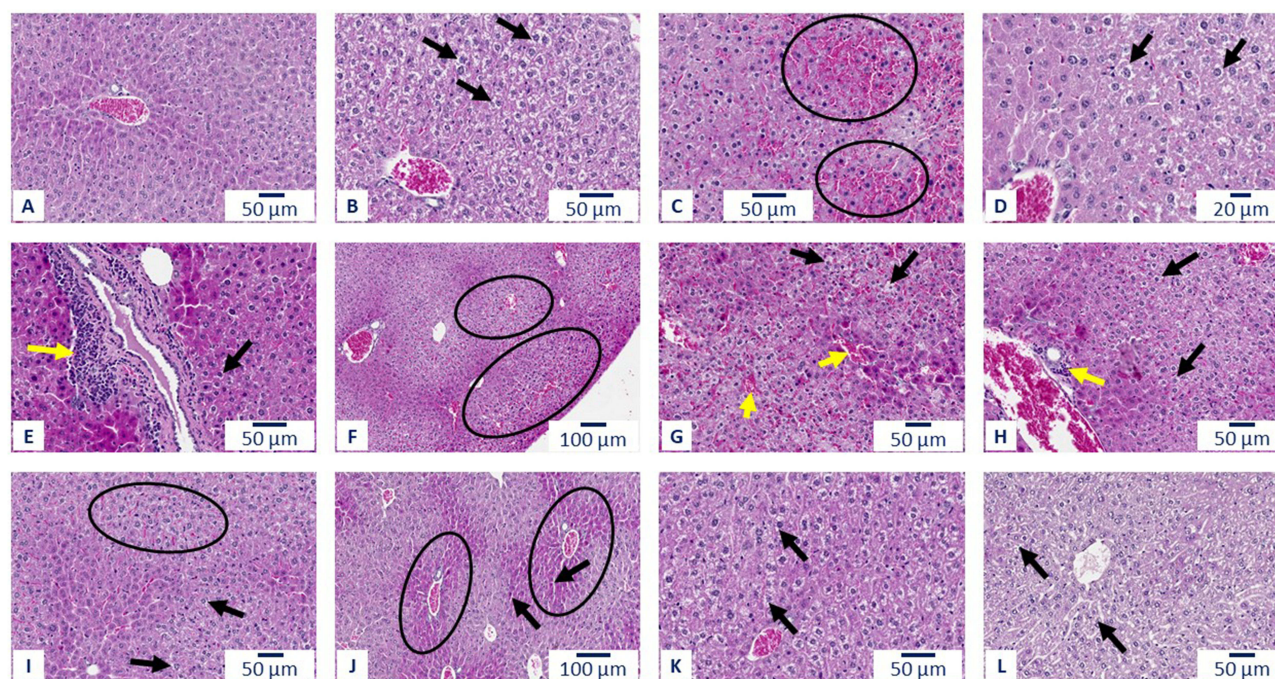
Figure 5 A photomicrograph of mice liver sections of control and different treatment groups. H&E staining. (**A**) Section of control group demonstrating normal liver architecture. (**B**) Sample of laser irradiation group presenting moderate cytoplasmic degeneration of hepatocytes (black arrows). (**C**) Laser irradiation group section revealing locally dilated and congested capillaries (black circles). (**D**) Section of DOX group demonstrating partially moderate cytoplasmic degeneration/vacuolization of hepatocytes (black arrows) (**E**) MPDAFe@Mem NPs group sample presenting slight cytoplasmic degeneration of hepatocytes (black arrow) and inflammatory infiltrations around bile ducts (yellow arrow). (**F**) Sample of MPDAFe@DOX@Mem NPs group presenting areas of liver with scattered hemorrhages (black circles). (**G**) MPDAFe@DOX@Mem NPs group section demonstrating dilated and congested sinusoids (yellow arrows) and vacuolated hepatocytes (black arrows). (**H**) MPDAFe@DOX@Mem NPs group sample revealing hepatocytes with cytoplasmic degeneration/vacuolization (black arrows), small inflammatory infiltrations around bile ducts (yellow arrow) (**I**) MPDAFe@Mem NPs and laser irradiation group section demonstrating areas with moderate, scattered hemorrhages (black circle) and slight degeneration/vacuolization of hepatocytes (black arrows). (**J**) DOX and laser irradiation group sample presenting dilated, but not congested sinusoids in the areas of portal triads (black arrows) and strong basophilic staining of regions around portal triads (black circles). (**K**) Section of MPDAFe@DOX@Mem NPs and laser irradiation group demonstrating cytoplasmic degeneration/vacuolization of hepatocytes (black arrows) (**L**) MPDAFe@DOX@Mem NPs and laser irradiation group sample revealing moderate cytoplasmic degeneration/vacuolization of hepatocytes (black arrows).

The kidney showed no changes in the structure. The histological structure was analogous to the control group (Figure 6B).

DOX Group

Cytoplasmic degeneration represented by vacuolization of hepatocytes was observed in small areas of the liver. Single binucleated hepatocytes are observed (Figure 5D).

In the kidney, partial injury of the epithelium is observed in some proximal tubules. Dilated venous system could be detected (Figure 6C and D).

MPDAFe@Mem NPs Group

Areas of hepatocytes with cytoplasmic degeneration were observed in the liver. Inflammatory infiltrates were visible around the bile ducts (Figure 5E).

Certain morphological changes were observed in kidney structure. Bowman's spaces in renal glomeruli were dilated. Flattening or vacuolization of some distal tubules was observed. Dilatation of the venous system referred to as venous congestion and edema around large veins were visible (Figure 6E–H).

MPDAFe@DOX@Mem NPs Group

Several hepatocytes exhibited cytoplasmic degeneration/vacuolization. Binucleated hepatocytes were present. Scattered hemorrhages were observed in areas with damaged hepatocytes, along with inflammatory cells infiltrations (Figure 5F–H).
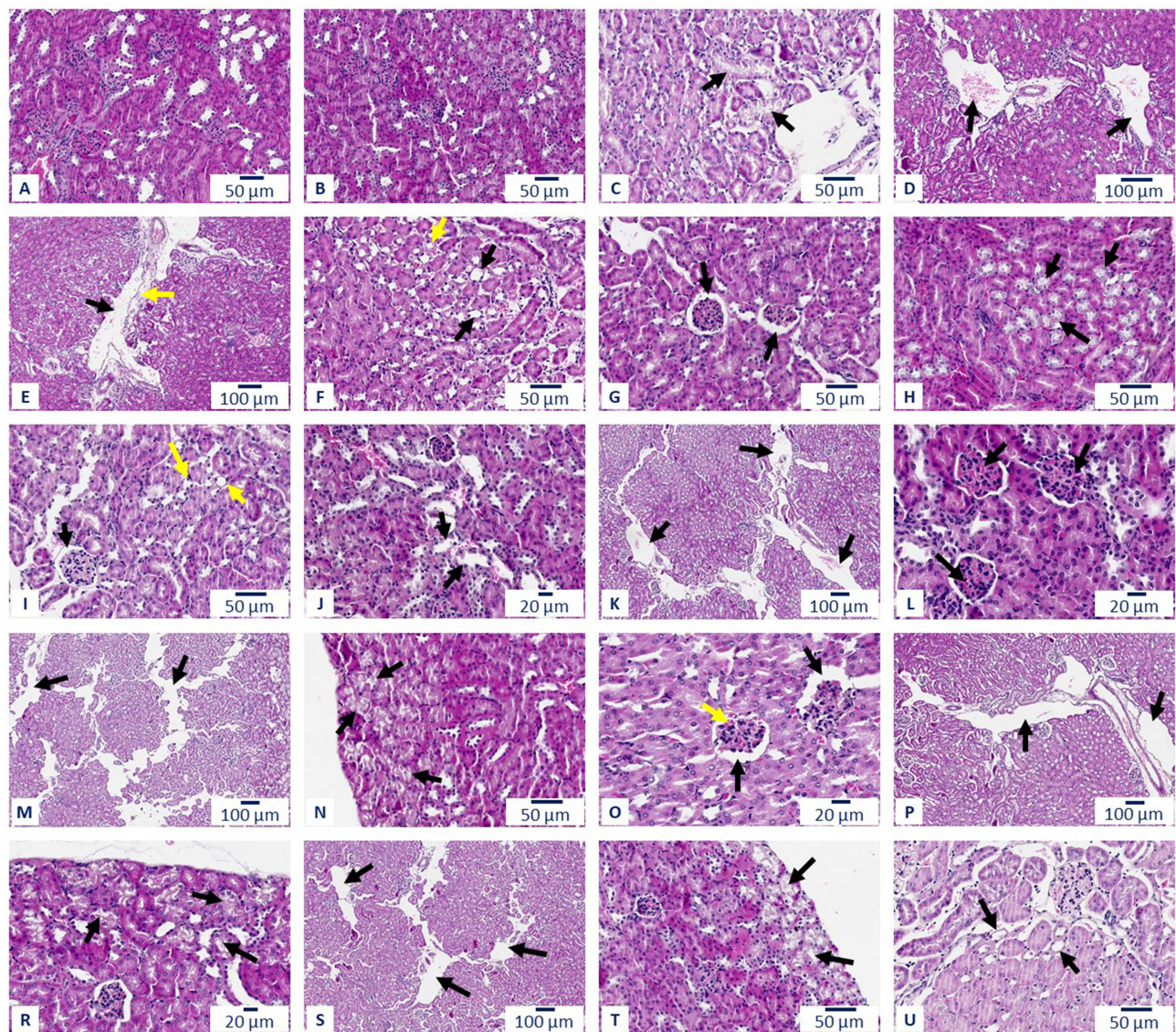
Figure 6 A photomicrograph of kidney sections presenting normal architecture in control group and structural changes in different treatment groups. H&E staining. (**A**) Control group sample demonstrating normal histological structure of kidney. (**B**) Kidney section of laser irradiation group revealing non-changed histological structure. (**C**) DOX group kidney sample demonstrating partially injured epithelium lining proximal tubules (black arrows). (**D**) DOX group kidney section presenting dilated veins (black arrows). (**E**) Section of MPDAFe@Mem NPs group demonstrating dilated veins (black arrow) with edema around large veins (yellow arrow). (**F**) MPDAFe@Mem NPs sample presenting partially flattened (black arrows) and partially vacuolated (yellow arrow) epithelium lining distal tubules. (**G**) MPDAFe@Mem NPs group section revealing widening of urinary space of glomerulus (black arrow). (**H**) Sample of MPDAFe@Mem NPs group demonstrating swollen, vacuolated epithelium of distal tubules (black arrows). (**I**) MPDAFe@DOX@Mem NPs group section demonstrating dilated Bowman's spaces (black arrow) and flattened epithelium of distal tubules (yellow arrows). (**J**) Section of MPDAFe@DOX@Mem NPs group presenting damaged epithelium of proximal tubules (black arrows). (**K**) MPDAFe@DOX@Mem NPs group section demonstrating dilated venous system (black arrows). (**L**) MPDAFe@DOX@Mem NPs group section revealing slightly dilated, congested capillaries of renal glomeruli (black arrows). (**M**) MPDAFe@Mem NPs and laser irradiation group sections presenting dilated veins (black arrows). (**N**) Sample of MPDAFe@Mem NPs and laser irradiation group demonstrating swollen and vacuolated epithelium lining proximal tubules localized in peripheral areas of kidney (black arrows). (**O**) Section of DOX and laser irradiation group revealing dilated Bowman's spaces (black arrows) and moderately congested glomeruli capillaries (yellow arrows). (**P**) Section of DOX and laser irradiation group demonstrating dilated veins (black arrow). (**R**) DOX and laser irradiation group sample presenting moderately swollen epithelium of proximal tubules of peripheral kidney regions (black arrows). (**S**) MPDAFe@DOX@Mem NPs and laser irradiation group section demonstrating dilated venous system (black arrows). (**T**) MPDAFe@DOX@Mem NPs and laser irradiation group section revealing vacuolated cells of proximal tubules epithelium localized in periphery of kidney. (**U**) Section of MPDAFe@DOX@Mem NPs and laser irradiation group presenting flattened epithelium of distal tubules.

In the kidney, a dilated and congested venous system, as well as dilated and congested capillaries in the renal glomeruli, were observed. The Bowman's spaces of glomeruli were dilated. Both proximal and distal tubules exhibited changes in epithelium (vacuolization, damage, flattening) (Figure 6I–L).

MPDAFe@Mem NPs and Laser Irradiation Group

Cytoplasmic degeneration of hepatocytes was observed in the liver, but it appear to be moderate. Moderate, scattered hemorrhages were visible in the peripheral part of the liver (Figure 5I).

Similar to previous groups, dilation of the venous system in the kidney was observed. Proximal tubules localized in the periphery of the kidney showed epithelium vacuolization (Figure 6M and N).

DOX and Laser Irradiation Group

Liver cells exhibited normal morphology. Cells around portal triads were stained strongly basophilically. Dilated, but not congested sinusoids in portal triad areas were observed (Figure 5J).

In the kidney, the venous system appears to be dilated. Glomeruli showed dilated Bowman's spaces and moderate congestion of capillaries. Epithelial vacuolization was visible in proximal tubules, especially in the peripheral part of the kidney (Figure 6O, P and R).

MPDAFe@DOX@Mem NPs and Laser Irradiation Group

The changes in the liver were limited to cytoplasmic degeneration of hepatocytes. Binucleated hepatocytes were also observed (Figure 5K and L).

The kidney showed the presence of significantly dilated veins. Peripheral proximal tubules contained vacuolization epithelium. Partially, the epithelium of distal tubules was flattened (Figure 6S–U).

Concentrations of Oxidative Stress Markers

Total Protein

The mean concentration of total protein for the liver was comparable among the individual groups (Figure 7A).

A significant increase in kidney TP level was observed in group VI treated with nanomaterials without drug (doxorubicin) but laser irradiated (25.05 ± 0.61 mg/mL), in comparison to group II treated only with nanomaterials without drug (21.89 ± 1.38 mg/mL), group III treated with doxorubicin (22.50 ± 0.85 mg/mL), group IV treated with
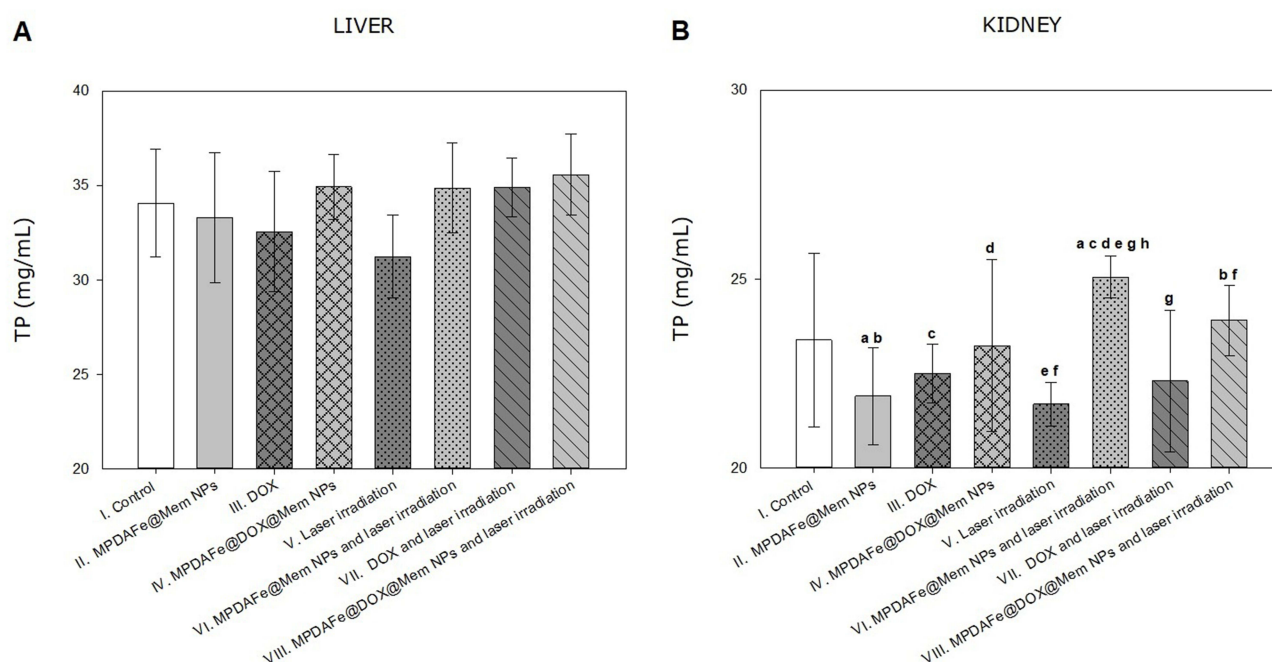

Figure 7 Comparison of TP concentrations in the liver (**A**) and kidney (**B**) of the control group (I) and animals exposed to MPDAFe@Mem NPs (group II), DOX (group III), MPDAFe@DOX@Mem NPs (group IV), laser irradiation (group V), MPDAFe@Mem NPs and laser irradiation (group VI), DOX and laser irradiation (group VII), MPDAFe@DOX@Mem NPs and laser irradiation (group VIII). Statistically significant results: a - groups significantly different at p = 0.0010; b - groups significantly different at p = 0.0303; c - groups significantly different at p = 0.0088; d - groups significantly different at p = 0.0490; e - groups significantly different at p = 0.0007; f - groups significantly different at p = 0.0220; g - groups significantly different at p = 0.0049.

polydopamine NPs loaded with doxorubicin (23.23 ± 2.46 mg/mL), group V laser irradiated (21.68 ± 0.58 mg/mL), group VII treated with DOX and laser irradiated (22.29 ± 2.04 mg/mL) and VIII treated with DOX-loaded MPDAFe NPs and laser irradiation (23.90 ± 1.02 mg/mL), as well as in group VIII treated with DOX-loaded MPDAFe NPs and laser irradiation (23.90 ± 1.02 mg/mL), in comparison to group II treated with treated only with nanomaterials without drug (21.89 ± 1.38 mg/mL), and group V treated with laser irradiation (21.68 ± 0.58 mg/mL) (Figure 7B).

Reduced Glutathione

In the case of the GSH level in the liver, statistically significant differences were noted (p = 0.0027); however, it was not possible to determine which groups differed (Figure 8A).

A significant increase in kidney GSH level was observed in group IV treated with polydopamine NPs loaded with doxorubicin (8.29 ± 2.97 nmol/mg) in comparison to group III treated with doxorubicin (6.07 ± 0.82 nmol/mg), V laser irradiated (5.71 ± 1.36 nmol/mg), and VII treated with DOX and laser irradiated (5.65 ± 1.48 nmol/mg).

In kidney of group IV treated with MPDAFe NPs loaded with doxorubicin (8.29 ± 2.97 nmol/mg), VI treated with nanomaterials without drug (doxorubicin) but laser irradiated (7.68 ± 2.44 nmol/mg), and VIII treated with DOX-loaded MPDAFe NPs and laser irradiation (6.77 ± 1.39 nmol/mg), a GSH level was significantly higher, than that observed in the control group I (4.74 ± 1.52 nmol/mg) (Figure 8B).

Nitrogen Oxide

No significant differences among the study groups were noted in liver and kidney NO (Figure 9A and B).

S-Nitrosothiols

In the case of the determined RSNO in the liver, no statistically significant differences were found (Figure 10A).

The RSNO level was significantly lower in kidney of group II treated with nanomaterials without drug (10.05 ± 1.85 nmol/mg), group III treated with doxorubicin (8.95 ± 3.44 nmol/mg) and group IV treated with DOX-loaded nanomaterials (9.90 ± 2.47 nmol/mg), compared to the control group I (12.40 ± 1.47 nmol/mg) (Figure 10B). Moreover, lower levels of kidney RSNO were observed in group III treated with doxorubicin (8.95 ± 3.44 nmol/mg), in comparison to
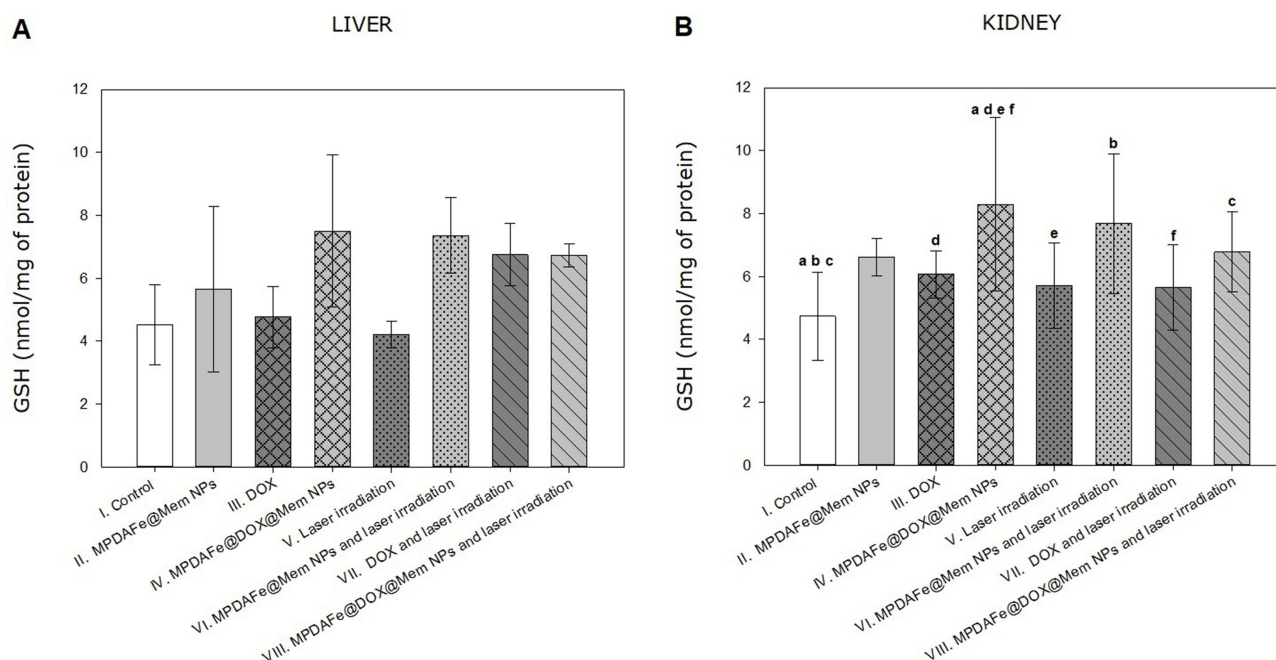

Figure 8 Comparison of GSH concentrations in the liver (**A**) and kidney (**B**) of the control group (I) and animals exposed to MPDAFe@Mem NPs (group II), DOX (group III), MPDAFe@DOX@Mem NPs (group IV), laser irradiation (group V), MPDAFe@Mem NPs and laser irradiation (group VI), DOX and laser irradiation (group VII), MPDAFe@DOX@Mem NPs and laser irradiation (group VIII). Statistically significant results: a - groups significantly different at p = 0.0005; b - groups significantly different at p = 0.0045; c - groups significantly different at p = 0.0445; d - groups significantly different at p = 0.0294; e - groups significantly different at p = 0.0121; f - groups significantly different at p = 0.0104.
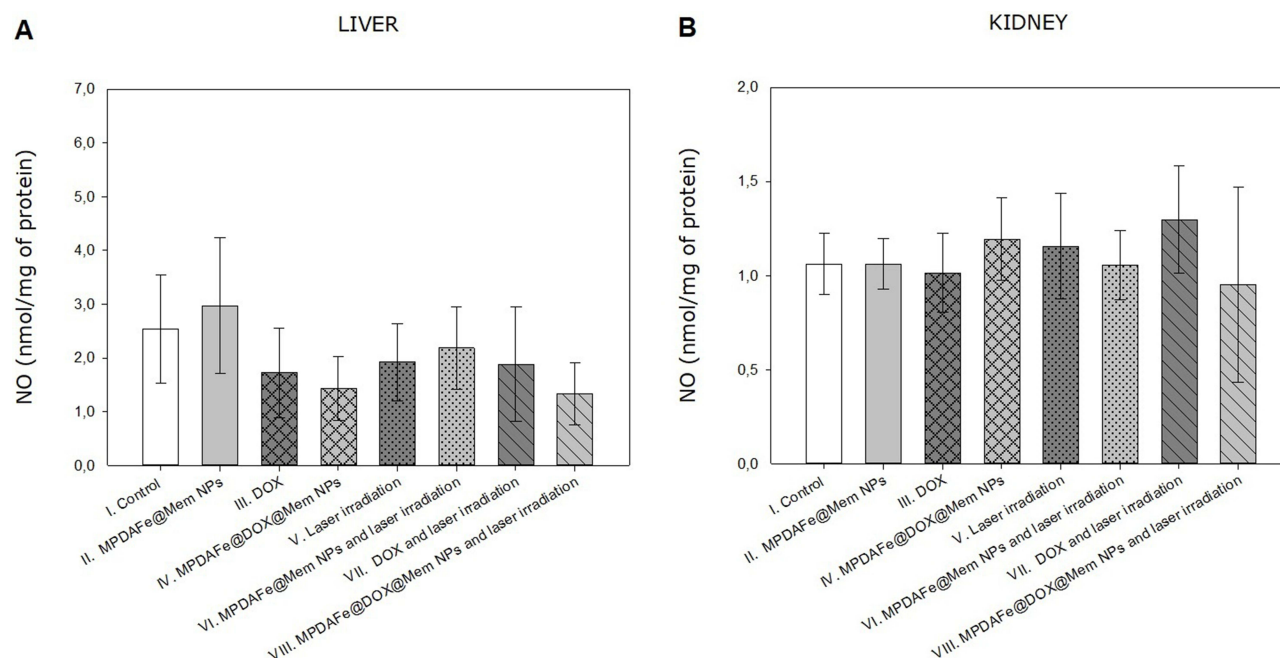
Figure 9 Comparison of NO concentrations in the liver (**A**) and kidney (**B**) of the control group (I) and animals exposed to MPDAFe@Mem NPs (group II), DOX (group III), MPDAFe@DOX@Mem NPs (group IV), laser irradiation (group V), MPDAFe@Mem NPs and laser irradiation (group VI), DOX and laser irradiation (group VII), MPDAFe@DOX@Mem NPs and laser irradiation (group VIII).
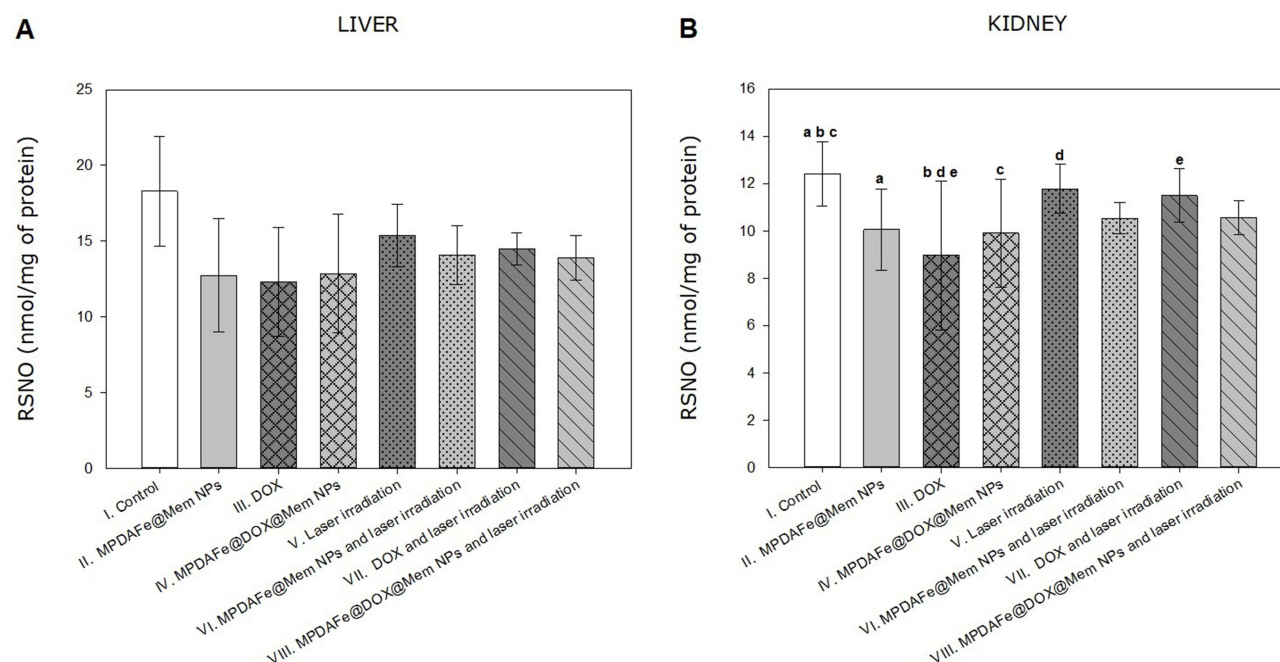

Figure 10 Comparison of RSNO concentrations in the liver (**A**) and kidneys (**B**) of the control group (I) and animals exposed to MPDAFe@Mem NPs (group II), DOX (group III), MPDAFe@DOX@Mem NPs (group IV), laser irradiation (group V), MPDAFe@Mem NPs and laser irradiation (group VI), DOX and laser irradiation (group VII), MPDAFe@DOX@Mem NPs and laser irradiation (group VIII). Statistically significant results: a - groups significantly different at p = 0.0016; b - groups significantly different at p = 0.0217; c - groups significantly different at p = 0.0150; d - groups significantly different at p = 0.0110; e - groups significantly different at p = 0.0219.

group V treated with laser irradiation (11.78 ± 1.02 nmol/mg) and group VII treated with DOX and laser irradiated (11.48 ± 1.24 nmol/mg).

Thiobarbituric Acid Reactive Substances

There was no statistically significant difference in liver TBARS levels between study groups (Figure 11A).

In the case of the kidney, a significantly higher levels of TBARS were observed among group IV treated with MPDAFe NPs loaded with doxorubicin (6.48 ± 1.01 nmol/mg), group VI treated with nanomaterials without drug (doxorubicin) but laser irradiated (6.31 ± 0.90 nmol/mg) and group VIII treated with DOX-loaded MPDAFe NPs and laser irradiation (6.80 ± 1.03 nmol/mg), compared to the control group I (5.14 ± 1.45 nmol/mg) (Figure 11B). Moreover, a significantly higher TBARS level was observed in the group VIII (6.80 ± 1.03 nmol/mg) in comparison to the group II (5.41 ± 1.29 nmol/mg).

Trolox Equivalent Antioxidant Capacity

The total antioxidant potential was significantly lower in the group VIII treated with DOX-loaded MPDAFe NPs and laser irradiation (24.43 ± 2.76 nmol/mg), compared to group IV treated with MPDAFe NPs loaded with doxorubicin (31.73 ± 2.85 nmol/mg), p = 0.0314 (Figure 12A).

No statistically significant differences were observed in the TEAC level in the kidney of the examined groups of animals (Figure 12B).

Catalase

The activity of CAT was significantly higher in the liver of the group VIII treated with DOX-loaded MPDAFe NPs and laser irradiation (205.66 ± 10.91 μmol/min/mg), compared to the control group I (114.97 ± 46.14 μmol/min/mg), group II treated only with nanomaterials without drug (146.77 ± 30.15 μmol/min/mg), and to group III treated with doxorubicin (152.13 ± 27.95 μmol/min/mg). Moreover, significantly higher CAT activity in the liver was noted in the group VI treated with nanomaterials without drug (doxorubicin) but laser irradiated (214.84 ± 28.83) in comparison to the control group I (114.97 ± 46.14 μmol/min/mg), and group II treated with MPDAFe NPs without drug (146.77 ± 30.15 μmol/min/mg) (Figure 13A).
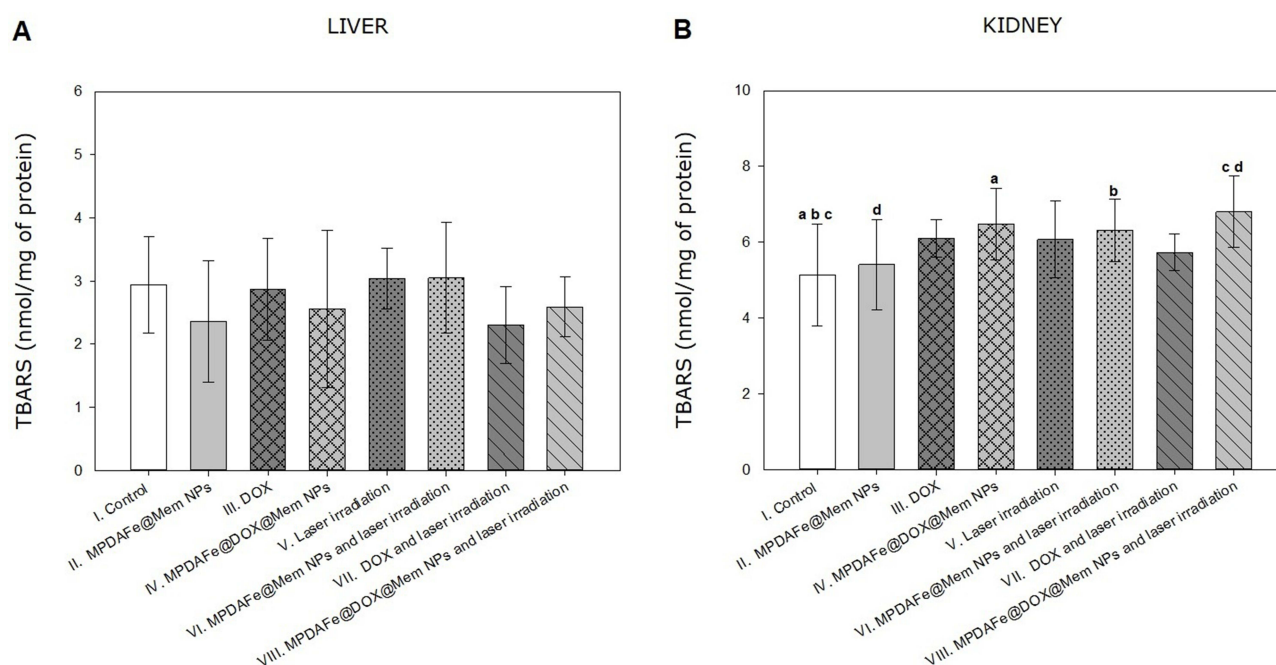

Figure 11 Comparison of TBARS concentrations in the liver (**A**) and kidney (**B**) of the control group (I) and animals exposed to MPDAFe@Mem NPs (group II), DOX (group III), MPDAFe@DOX@Mem NPs (group IV), laser irradiation (group V), MPDAFe@Mem NPs and laser irradiation (group VI), DOX and laser irradiation (group VII), MPDAFe@DOX@Mem NPs and laser irradiation (group VIII). Statistically significant results: a - groups significantly different at p = 0.0180; b - groups significantly different at p = 0.0457; c - groups significantly different at p = 0.0054; d - groups significantly different at p = 0.0182.
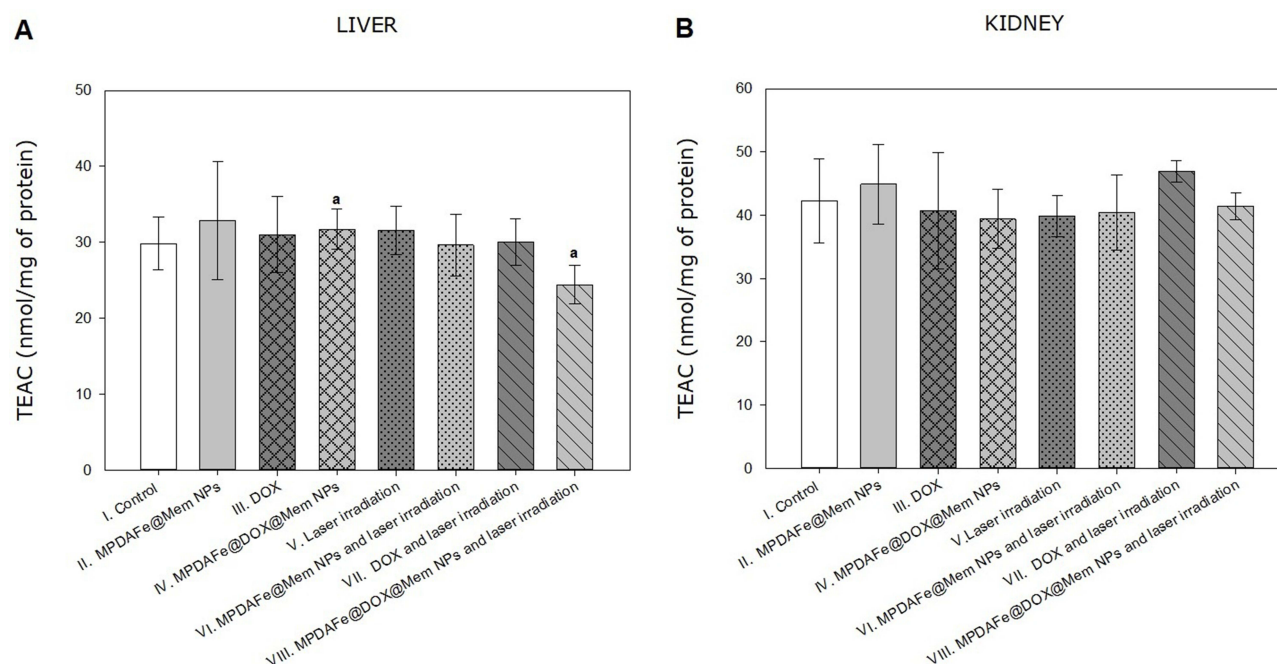
Figure 12 Comparison of TEAC concentrations in the liver (**A**) and kidney (**B**) of the control group (I) and animals exposed to MPDAFe@Mem NPs (group II), DOX (group III), MPDAFe@DOX@Mem NPs (group IV), laser irradiation (group V), MPDAFe@Mem NPs and laser irradiation (group VI), DOX and laser irradiation (group VII), MPDAFe@DOX@Mem NPs and laser irradiation (group VIII). Statistically significant results: a - groups significantly different at p = 0.0314.
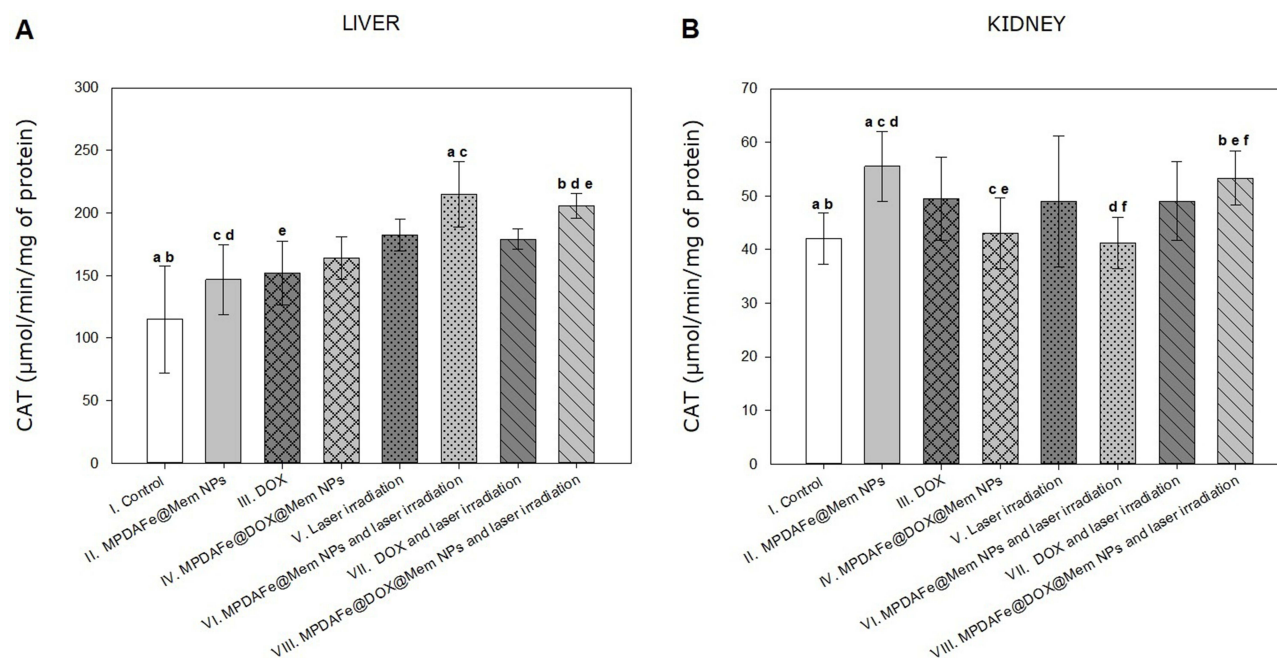

Figure 13 Comparison of CAT activity in the liver (**A**) and kidney (**B**) of the control group (I) and animals exposed to MPDAFe@Mem NPs (group II), DOX (group III), MPDAFe@DOX@Mem NPs (group IV), laser irradiation (group V), MPDAFe@Mem NPs and laser irradiation (group VI), DOX and laser irradiation (group VII), MPDAFe@DOX@Mem NPs and laser irradiation (group VIII). Statistically significant results in liver: a - groups significantly different at p = 0.0007; b - groups significantly different at p = 0.0004; c - groups significantly different at p = 0.0355; d - groups significantly different at p = 0.0145; e - groups significantly different at p = 0.0090. Statistically significant results in kidney: a - groups significantly different at p = 0.0027; b - groups significantly different at p = 0.0143; c - groups significantly different at p = 0.0052; d - groups significantly different at p = 0.0023; e - groups significantly different at p = 0.0251; f - groups significantly different at p = 0.0117.

The activity of CAT was significantly higher in the kidney of the group II treated with nanomaterials without drug (55.56 ± 7.01 µmol/min/mg), and VIII treated with DOX-loaded MPDAFe NPs and laser irradiation (53.33 ± 5.55 µmol/min/mg), compared to group I (42.06 ± 5.22 µmol/min/mg), group IV treated with MPDAFe NPs loaded with doxorubicin (43.07 ± 7.19 µmol/min/mg) and group VI treated with nanomaterials without drug (doxorubicin) but laser irradiated (41.27 ± 5.28 µmol/min/mg) (Figure 13B).

Glutathione S-Transferase

No statistically significant differences were observed in the liver among individual study groups in the case of GST (Figure 14A).

A significantly lower level of GST activity in the kidney was noted for group VI treated with nanomaterials without the drug (doxorubicin) but laser irradiated (12.07 ± 4.26 nmol/min/mg), compared to group II treated with nanomaterials without the drug (29.05 ± 6.93 nmol/min/mg) (Figure 14B).

Superoxide Dismutase

A statistically significant difference in the liver SOD activity (Figure 15A) was demonstrated between group V laser irradiated (4.59 ± 0.50 U/mg) and group VII treated with DOX and laser irradiated (3.53 ± 0.70 U/mg).

The activity of SOD was significantly lower in the kidney of the group VI treated with nanomaterials without drug (doxorubicin) but laser irradiated (2.77 ± 0.16 U/mg), VII treated with DOX and laser irradiated (2.80 ± 0.28 U/mg), and VIII treated with DOX-loaded MPDAFe NPs and laser irradiation (2.78 ± 0.20 U/mg) compared to the control group I (3.47 ± 0.26 U/mg) (Figure 15B).

Discussion

Cancer cells produce greater amounts of ROS due to their high metabolic rate; however, similar to healthy cells, they maintain redox homeostasis by balancing ROS production with adequate levels of antioxidants. In both healthy and cancer cells, when this balance is not maintained, oxidative stress occurs, leading to cell death.[40] The so-called "oxidative therapy" may be a form of cancer treatment, involving the induction of cytotoxic oxidative stress.[41] Anti-cancer therapies often use pro-oxidant chemotherapy drugs, such as cisplatin, doxorubicin, or ionizing radiation to induce oxidative
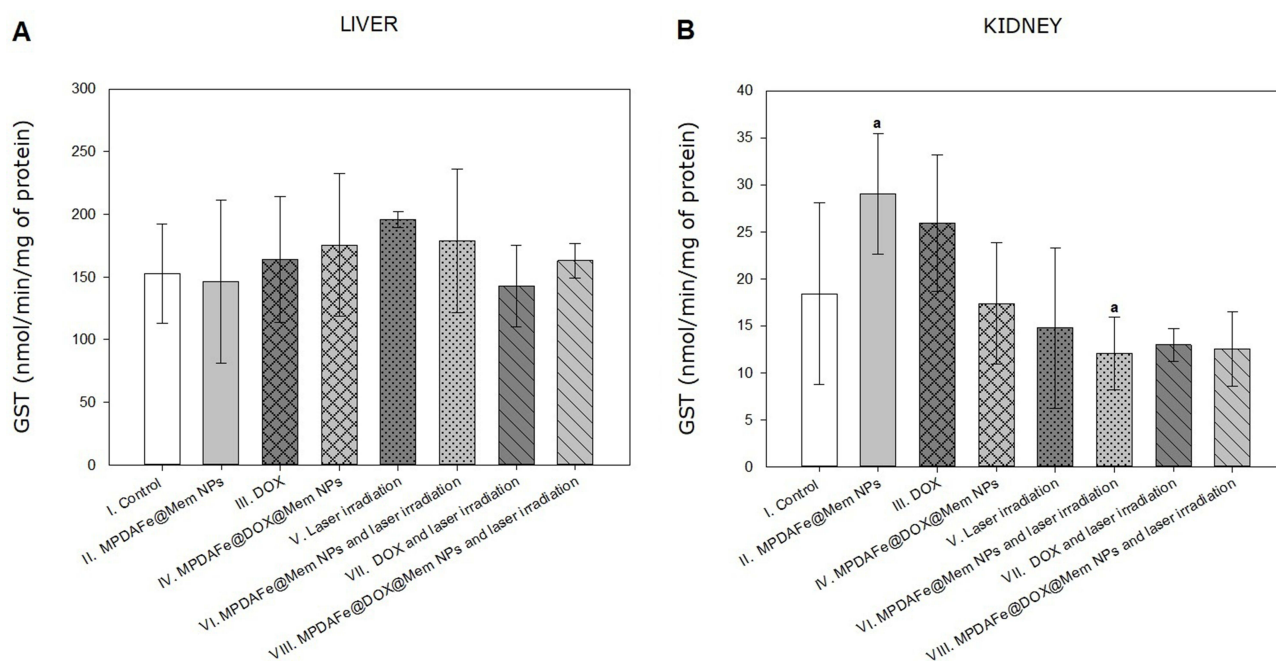

Figure 14 Comparison of GST activity in the liver (**A**) and kidney (**B**) of the control group (I) and animals exposed to MPDAFe@Mem NPs (group II), DOX (group III), MPDAFe@DOX@Mem NPs (group IV), laser irradiation (group V), MPDAFe@Mem NPs and laser irradiation (group VI), DOX and laser irradiation (group VII), MPDAFe@DOX@Mem NPs and laser irradiation (group VIII). Statistically significant results: a - groups significantly different at p = 0.0239.
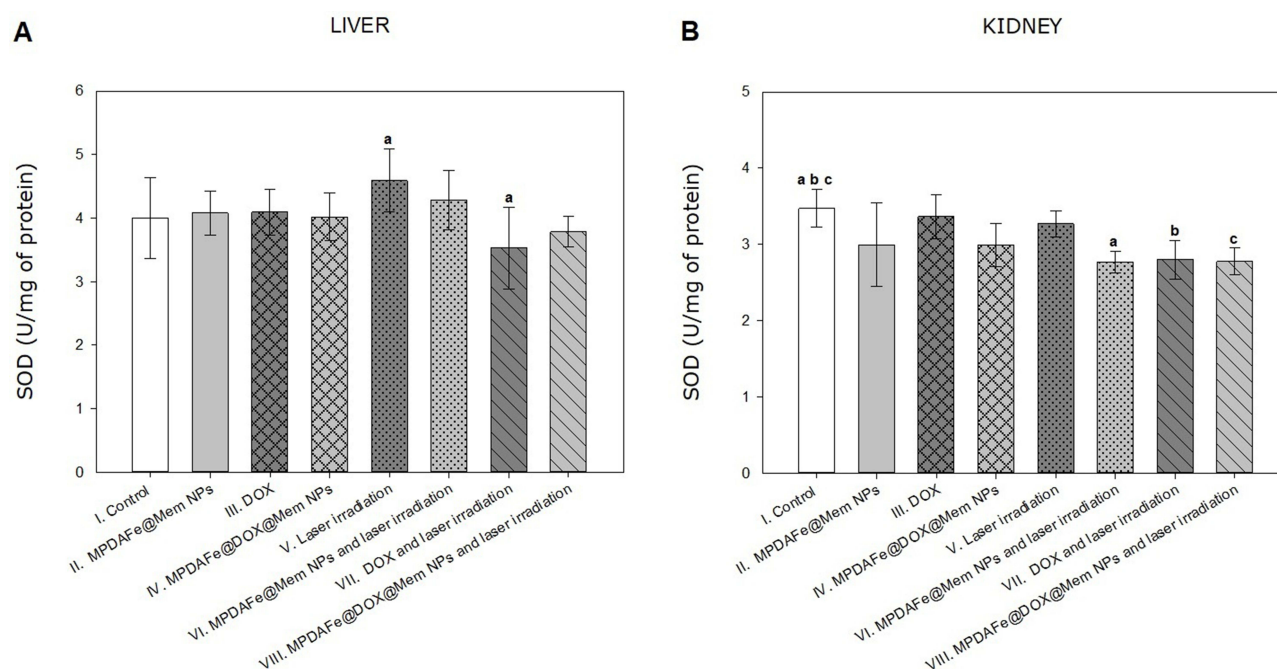
Figure 15 Comparison of SOD activity in the liver (**A**) and kidney (**B**) of the control group (I) and animals exposed to MPDAFe@Mem NPs (group II), DOX (group III), MPDAFe@DOX@Mem NPs (group IV), laser irradiation (group V), MPDAFe@Mem NPs and laser irradiation (group VI), DOX and laser irradiation (group VII), MPDAFe@DOX@Mem NPs and laser irradiation (group VIII). Statistically significant results in liver: a - groups significantly different at p = 0.0334. Statistically significant results in kidney: a - groups significantly different at p = 0.0055; b - groups significantly different at p = 0.0308; c - groups significantly different at p = 0.0109.

stress.[42] Unfortunately, this strategy causes an increase in antioxidant defense over time and leads to the emergence of chemoresistance.[40,43,44] Another problematic issue is the extreme toxicity of chemotherapy drugs.[45]

Polydopamine is a melanin-like material formed through the oxidation and polymerization of dopamine upon exposure to atmospheric oxygen in alkaline aqueous conditions. Polydopamine and melanin are structurally similar; therefore, both have similar physicochemical properties.[46] Indeed, nanoparticles based on polydopamine have been reported to display good antioxidant properties, although their efficacy and mechanism of action are still unclear.[30,47–49] In recent years, researchers have mainly focused on the application of PDA NPs, especially for cancer treatment and diagnostic purposes.-[26,29,50] Nevertheless, to date, few studies have explored the potential toxicity study of MPDA, which hampers further clinical application.

In this study, we aimed to evaluate the potential toxicity of mesoporous polydopamine nanoparticles modified with iron coated with cancer cell membrane and loaded with doxorubicin (MPDAFe@DOX@Mem NPs). This was assessed through histological evaluation of tissues and the analysis of oxidative stress biomarkers in the liver and kidney of BALB/c nude mice with xenograft human hepatoma HepG2 cells, subjected to CT-PTT. Although in vivo studies with Balb/c nude mice yielded somewhat inconclusive results, they provide a valuable reference for future investigations.

Body and organ weights are important indicators for early toxicity. Silva et al described that 5% body weight loss is a strong empirical of pathological findings.[51] During our experiment, beyond the control group, no significant decreases in body weight were observed among study groups, as mice lost no more than 5% of their body weight throughout the study. Additionally, there were no differences in organ weights (liver, right kidney, left kidney, heart, brain, lungs, pancreas, spleen) between the study groups. Clinical symptoms were stable throughout the treatment period.

Following the administration of a single dose of MPDAFe@DOX@Mem into the tail vein and subsequent laser irradiation, histological changes in the liver were limited to cytoplasmic degeneration of hepatocytes and the presence of binucleated hepatocytes. In the kidneys, significantly dilated veins were observed, along with vacuolization in the epithelium of the peripheral proximal tubules and partially flattened epithelium of the distal tubules. Kuthati et al demonstrated that mesoporous polydopamine nanoparticles loaded with morphine (MPDA@Mor) had a significant

hepatoprotective effect in relation to morphine-induced hepatotoxicity by suppressing liver enzymes (ALT, AST, LDH), as confirmed by histological tests.[52]

When introduced into the body, polydopamine nanomaterials due to numerous catechol structures, display a strong adhesion ability, therefore can readily interact with blood proteins and form protein corona.[53] Various factors and protein–NP interactions in vivo can induce changes in protein conformation and as a result, change the further functionality and affect their stability, and bioactivity, hindering the transfer efficiency to tumors and reducing the bioavailability.[54,55] In this study, we examined total protein levels in liver and kidney homogenates of mice intravenously administered with MPDAFe@ NPs (4.44 mg/kg bw) loaded with DOX (2 mg/kg bw). The mean liver total protein concentration was comparable across the groups. However, a significant about 8–14% increase in kidney TP levels was observed in the group treated with MPDAFe@Mem NPs without DOX subjected to laser irradiation, in comparison to all experimental groups, as well as in group treated with MPDAFe@DOX@Mem NPs and laser irradiated, in comparison to the group treated with MPDAFe@Mem NPs, or group exposed only to laser irradiation. This suggests that PTT had a significant impact on the increase in TP levels in the groups administered MPDAFe NPs. In a similar experiment using Balb/c mice, Zhang et al did not observe any significant difference of total protein concentrations in serum between the control group and group of animals injected into the tail vein with polydopamine/mesoporous calcium phosphate hollow Janus nanoparticles functionalized with indocyanine green and methoxy-poly(ethylene glycol)thiol (PEG-ICG PDA/mCaP H-JNPs) at a dose of 20 mg/kg.[56] Li et al have tested markers of liver function, including total protein among mice treated with polydopamine labeled with arginine-glycine-aspartic-cysteine acid with doxorubicin (PDA-RGDC-DOX) by intravenous injection at a concentration of 2 mg/mL and irradiated with the 808 nm laser at the power intensity of 2 W/cm^2 for 5 min. No statistically significant differences were observed in the total protein levels in the livers of mice, compared to the control group after a month of study.[57] Furthermore, Witkowska et al showed no statistically significant differences in total protein concentrations in the homogenates of the liver, kidneys, and brain of nude mice from the control group, group injected one time into the tail vain with PDA nanoparticles coated with PAMAM dendrimers and functionalized with folic acid by PEG linker (PDA@DG3@PEG@FA), and group administered PDA@DG3@PEG@FA with encapsulated doxorubicin (PDA@DG3@PEG@FA@DOX) (where the dose corresponded to 35 mg/kg bw of PDA and 15 mg/kg bw of DOX), exposed to the 808 nm laser at a power intensity of 1 W/cm^2 for 5 min.[26]

Glutathione is an important component of the antioxidant system, widely distributed in our body.[40,58] Studies have shown that GSH performs both protective and pathogenic roles. In healthy cells, it detoxifies xenobiotics and carcinogens. Its decrease contributes to oxidative stress implicated in the progression of cancer. In many cancer cells (ie bone marrow, breast, colon, hepatocarcinoma, melanoma, lung, and pancreatic cancer), elevated GSH levels increase the cells' resistance to oxidative stress and may indirectly contribute to tumor progression and increase resistance to chemotherapy drugs.[40] Multidrug resistance and the role of glutathione in this phenomenon is the object of interest of many scientists. It has been shown that treatment with the anticancer drug doxorubicin reduces GSH levels in cancer cells.[59,60] Glutathione depletion induced by erastin leads to significantly higher cytotoxicity of cisplatin and reduced tumor resistance to this chemotherapy.[61,62] In contrast, exogenous GSH in combination with DOX significantly reduce the anticancer efficacy of DOX in a dose-dependent manner as confirmed by investigation in xenograft nude mice and cancer cell models, including MCF-7, HepG2, and Caco-2 cells.[63] Moreover, the same study proved that exogenous GSH increases intracellular GSH levels, thereby reducing the side effects of DOX, which include hepatotoxicity and cardiotoxicity.[63] Feng et al administered polydopamine at a dose of 1 mg/mL into the tumor together with the photosensitizer, L-arginine, and methylene blue, and observed a 21% reduction in GSH levels compared to the control group.[64] Witkowska et al have shown that mean GSH concentration in the liver homogenate of Balb/c mice from the group treated with PDA@DG3@PEG@FA@DOX and PTT was significantly 31% lower than the values obtained in the control group. Statistically important 45.54% decrease of GSH was observed also in the brain of animals from the PDA@DG3@PEG@FA group compared to animals from the control group, however in the group administered PDA@DG3@PEG@FA@DOX and laser irradiated was observed a significant increase of 140% in GSH concentration in comparison to the PDA@DG3@PEG@FA group.[26] In our study, we have observed an increase of GSH levels in the kidneys of mice from the group treated with polydopamine nanoparticles loaded with doxorubicin (MPDAFe@DOX@Mem NPs) (by 75%), the group treated with nanomaterials without drug (MPDAFe@Mem NPs) but laser irradiated (by 62%), and group treated with DOX-loaded MPDAFe@Mem NPs and laser irradiation (by 43%), compared

to the control group. To summarize, in the kidneys of groups subjected to therapies in combination with MPDAFe nanoparticles, the concentration of glutathione was higher than in the analogous groups without PDA, although this effect was suppressed when therapy was combined with laser irradiation.

Glutathione S-transferase is a GSH-dependent enzyme that protects cells by neutralizing (reducing) reactive oxygen species.[65] This enzyme catalyzes the conjugation of GSH with drugs (eg cisplatin) and facilitates the efflux of drugs through membrane transporters (multidrug resistance proteins), the increased expression of which may be associated with the acquisition of resistance to chemotherapy.[66] The detoxifying function of GST affects the second phase of xenobiotics detoxication and some carcinogens and cytotoxic products of lipid peroxidation.[39,67] In our study, we observed a significant decrease of approximately 58% in GST activity in the kidneys of the group treated with nanomaterials without the drug (doxorubicin) but laser irradiated, compared to the group treated with nanomaterials without the drug. However, Witkowska et al demonstrated that the activity of GST in the brains of mice receiving PDA@DG3@PEG@FA@DOX nanoparticles and subjected to phototherapy was 72% higher compared to the group receiving only PDA@DG3@PEG@FA nanoparticles.[26] Cancer tumors are also characterized by an increased occurrence of reactive nitrogen species (RNS). The best-known RNS form is nitric oxide, a membrane-soluble free radical, synthesized by nitric oxide synthase (NOS) in tumor stromal cells or infiltrating immune cells. Nitric oxide is an important oxidative biological signaling molecule and has both a pro-oxidant and antioxidant properties.[68] The pathogenic potential of NO largely depends on its concentration and its proximity to ROS, such as superoxide. At lower concentrations, NO directly affects processes like proliferation and cell survival, while at higher concentrations, it leads to nitrosative modifications of proteins and lipids. RNS-dependent modifications include post-translational protein modifications, nitration and S-nitrosylation. Nitration concerns aromatic amino acids such as tyrosine and tryptophan, whereas S-nitrosylation occurs by covalently attaching the nitrosyl group to the sulfur atom of cysteine, which contains a sulfhydryl group (-SH).[62] An increased content of nitrated proteins was observed during pathophysiological processes such as inflammation, atherosclerosis, neurodegenerative and cardiovascular diseases.[68] Data show that lipid peroxyl radicals (LOO•) promote nitration in some cases. In turn, S-nitrosylation is a modification that reversibly changes the functions of many proteins and is classified as a signaling transformation. Under physiological conditions, during S-nitrosylation of proteins, stable nitrosothiols are formed, protecting -SH groups against irreversible modifications.[68,69] However, existing evidence suggests that in the presence of excessive RNS production, such mechanisms may lead to the loss of biomolecule function, disruptions in protein function, mitochondrial dynamics, protein folding in the ER, and signaling pathways, which contribute to synaptic damage, neurodegeneration, and even cell death.[70] Our results indicate that no statistically significant differences were found in RSNO levels in the liver. However, the RSNO level was significantly lower in the kidney of the group treated with nanomaterials with or without the drug (by around 20% both) and with doxorubicin only (by 28%), compared to the control group. Additionally, lower levels of kidney RSNO were observed in the group treated with doxorubicin, in comparison to the group treated with laser irradiation and the group treated with DOX and laser irradiation (by around 30% both). In our study, no significant differences were noted in liver and kidney NO levels among the study groups.

Reactive oxygen species can react with polyunsaturated fatty acids in cellular membranes, lipoproteins, and other molecules that contain lipids, inducing lipid peroxidation, which is quantified as the concentration of thiobarbituric acid reactive substances (TBARS).[41] It has been shown that the level of lipid peroxidation products in hepatoma cells was lower than in normal liver cells.[41] Canuto et al demonstrated that during rat liver carcinogenesis, the activity of aldehyde-metabolizing enzymes increased, which provided cancer cells with better protection against the cytotoxic effects of aldehydes.[71] Furthermore, in hepatoma cells, most of the lipid peroxidation end-products, such as 4-hydroxynonenal (HNE), are converted to HNE-GSH conjugates and rapidly exported out of the cell.[41] Elevated levels of malondialdehyde (MDA) and TBARS are important markers of oxidative stress in biological material.[72] Uncontrolled iron-mediated lipid peroxidation of cell membranes leads to the accumulation of lipid hydroperoxides, ultimately causing cell death through a recently discovered cell death pathway called ferroptosis, which is associated with both neurodegenerative diseases and tumor suppression.[73] Zhang et al proved that PDA NP ($\approx$ 220 nm) can chelate Fe^{2+} ions and scavenge-free radicals, thereby protecting the heart from ischemia-reperfusion damage by inhibiting ferroptosis.[74] Similarly, Lei et al synthetized curcumin–polydopamine nanoparticles (Cur–PDA NPs) with the ability to inhibit ferroptosis by chelating both Fe^{2+} and

Fe^{3+} and scavenging free radicals.[75] On the other hand, Yu et al developed tumor-targeted nanoparticles composed of iron-polydopamine, folic acid-modified red blood cell membrane, and epirubicin (Fe-PDA-EPI@FA-RBCm NPs), in the context of an anticancer strategy using the enhanced photothermo-ferroptosis effect. Their study showed that these biomimetic nanoparticles can participate in the formation of hydroxyl radicals ($\cdot$OH) from the decomposition of hydrogen peroxide (H_2O_2) through the iron-catalyzed Fenton reaction, leading to the activation of the non-apoptotic ferroptosis pathway. Phototherapy further intensified ferroptosis by increasing the production of ROS and lipid peroxides and by reducing the expression of glutathione peroxidase 4 (GPX4) and the mitochondrial membrane potential.[76] Ding et al developed mesoporous Fe_3O_4 NPs loaded with pyropheophorbide-a (ppa), coated with polydopamine and anchored with tumor-targeted biotin moieties (Fe/ppa@PDA/B NP). These nanoparticles induced synergistic apoptosis and ferroptosis through GSH depletion and the action SOD in sonodynamic therapy (SDT).[77] Kuthati et al studied mesoporous polydopamine nanoparticles loaded with morphine (MPDA@Mor) in 7-week-old Wistar rats with partial sciatic nerve transection to induce neuropathic pain. They observed a 24% higher MDA level in liver homogenates than in the sham animals, while the group treated with morphine had a 36% lower MDA level. Treatment with MPDA@Mor significantly attenuated the suppression also of hepatic antioxidant enzymes, SOD and CAT, which suggests that delivery of morphine with an antioxidant nanocarrier can reduce the hepatic oxidative stress caused by morphine administration.[52] Wikowska et al observed statistically significant higher TBARS levels in the liver and kidney of mice administered PDA@DG3@PEG@FA (by 52% and 59%), and in the group treated with PDA@DG3@PEG@FA@DOX and irradiated with laser (by 42% in the liver; by 38% in the kidney) compared to the control group. Similarly, in our study, significantly higher TBARS levels (23–32%) were observed in kidneys of animals administrated with DOX-loaded MPDAFe NPs, with or without photothermal therapy (PTT), compared to the control group. However, no statistically significant differences in liver TBARS levels were observed across the study groups.

By reacting with free radicals, NO inhibits lipid peroxidation, while in the presence of O2•−, NO is converted to peroxynitrite (ONOO-), a strong biological oxidant.[69] The concentration of O2•− in the cell is strictly controlled by SOD activity, which catalyzes the dismutation of O2•− into molecular oxygen (O_2) and hydrogen peroxide (H_2O_2). The formation of ONOO- intensifies when the SOD activity is low, and SOD deficiency under conditions of increased oxidative stress may contribute to early cancer development.[49] In our study, SOD activity was significantly (around 20%) lower in the kidney of mice from the groups subjected to laser irradiation which were treated before with DOX, nanomaterials without the drug (doxorubicin), or DOX-loaded MPDAFe NPs, compared to the control group. We also observed a 23% decrease in SOD activity in the liver of doxorubicin-treated animals that were irradiated, compared to the laser-only group.

Hu et al confirmed that adding palladium (Pd) to PDA enhances its ROS-scavenging effects, because Pd nanoparticles have good CAT-like enzyme and SOD-like enzyme activities, thus, can scavenge hydroxyl radicals and superoxide anions. Moreover, the same study confirmed that NIR significantly promotes the catalase-like activity of PDA-Pd NPs.[78]

Catalase is a tetrameric ferriheme oxidoreductase that is mainly located in peroxisomes and that is most active in the liver and red blood cells.[49] It plays an important role in cancer by scavenging high concentrations of H_2O_2 and protecting cell wall lipids and lipoproteins from peroxidation.[79,80] Moreover, cancer cells contribute to changing the expression of catalase, which plays a double role in cancer processes.[81] Catalase can limit cancer initiation by ROS accumulation, but some cancer types, such as melanoma and glioblastoma multiforme, require increased catalase activity to balance ROS production and prevent apoptosis.[80] It has been proven that catalase limits the apoptosis of HepG2 liver cancer cells caused by the administration of DNA-damaging cytostatic by reducing the level of p53, a tumor suppressor protein.[82] Our study has shown that the activity of CAT significantly increases in the liver and kidney of the group treated with DOX-loaded MPDAFe NPs coated with cancer cell membrane and subjected to laser irradiation. This contrasts with the study by Witkowska et al, which showed a significant decrease in kidney CAT activity was noted in the group of animals receiving the DOX-loaded PDA NPs with PAMAM dendrimers functionalized with folic acid combined with PTT compared to the control group.[26]

Trolox equivalent antioxidant capacity (TEAC) assay measures the total antioxidant capacity (TAC) of a substance, using Trolox, a synthetic derivative of vitamin E, as a standard.[83] Witkowska et al showed that that animals treated with PDA@DG3@PEG@FA exhibited a significant decrease in TEAC levels in kidney homogenate compared to the control group (p = 0.008034). In studies on polydopamine-based immunosuppressive nanoparticles with potential in the

treatment of ischemic stroke, Shi et al demonstrated their concentration-dependent antioxidant properties.[84] O'Connor et al analyzed hydrogels containing polydopamine in various concentrations in terms of their ability to reduce the ABTS • + cation radical in relation to Trolox. The study observed that as the concentration of PDA in the hydrogel increased, the percentage of reduced ABTS increased.[85] In our research, we observed that the total antioxidant potential was significantly lower (by 23%) in the group treated with laser 24 h after DOX-loaded MPDAFe NPs administration, compared to those treated with DOX-loaded MPDAFe NPs alone (p = 0.0314). We did not observe any significant differences in TEAC in kidneys among the analyzed groups.

One of the main challenges with using metal-containing nanomaterials in medical applications is their poor biocompatibility and biodegradability. To overcome this limitation, materials such as polydopamine are used to improve bioavailability.[14,48] Among numerous ROS-scavenging materials, PDA has attracted much attention due to its excellent ROS scavenging ability and biocompatibility. Although PDA, as an antioxidant, also has some disadvantages as a therapeutic. Antioxidants scavenge ROS through direct redox reactions, and the content of their reducing groups is gradually consumed with the clearance of ROS. Therefore, their effective therapeutic concentration is difficult to maintain for a long time and repeated administration is advisable, which is a significant difficulty in practical application.[78]

In recent years, research on the use of PDA nanoparticles in biological applications has been widely conducted. However, the safe use of polydopamine in medicine is still hindered by limited knowledge of its toxic effects. When assessing the toxicity of PDA nanoparticles, several factors, such as size, shape, and modifications, must be considered, as nanoparticles can produce different toxic effects in vivo.[19] Carmignani et al demonstrated the effect of NPs size on the PDA antioxidant activity (from 150 to 960 nm). The scavenging efficiency of OH· radicals decreased rapidly, with the increase of PDA NPs size (92.2–10%).[86]

The great potential of PDA nanomaterials, proven in in vitro studies, requires confirmation in in vivo studies so that their properties can be exploited in clinical trials in the future. In vivo, nanoparticles encounter a complex environment that cannot be replicated in vitro.[54] Deciphering complex nano-bio interactions and understanding the connections between the different physicochemical properties of nanoparticles is crucial for the development of nanomedicine. Furthermore, due to many experimental factors that may ultimately influence the research results, there is an increasing need for standardization in this field. Currently, there is still a lack of sufficient research on the toxicity and safety of new PDA nanomaterials. Chronic toxicity tests are also necessary to observe potential in vivo changes with long-term exposure. In the present study, no significant differences between the study groups concerning tumor growth inhibition were observed. However, to our knowledge, there are no such comprehensive reports on the impact of PDA nanomaterials on the antioxidant-pro-oxidant balance and in vivo organ toxicity to date.

Although the anticancer effectiveness in vivo studies with Balb/c nude mice yielded quite ambiguous results, they can serve as a valuable reference point for future investigations. Understanding the mechanisms of oxidative stress resulting from the use of PDA NPs in combination with combined chemo- and photothermal therapy in cancer treatment may improve existing therapies of liver cancer and create new strategies to improve therapeutic outcomes and alleviate the toxic and side effects of chemotherapy drugs. Therefore, the presented data has translational potential of PDA materials in future anticancer therapies.

Conclusion

1. The tested mesoporous polydopamine nanoparticles modified with iron and coated with cancer cell membrane and loaded with doxorubicin (MPDAFe@DOX@Mem NPs) combined with photothermal therapy (CT-PTT) did not cause any significant decrease in the body weight of mice throughout the study. There were no differences in average organ weights (liver, right kidney, left kidney, heart, brain, lungs, pancreas, spleen) between the study groups. The clinical symptoms were stable throughout the whole treatment period.

2. After a single dose of MPDAFe@DOX@Mem administered into the tail vein and laser irradiation, histological changes in the liver showed cytoplasmic degeneration of hepatocytes and binucleated hepatocytes appeared. In the kidneys, significantly dilated veins were noted, along with vacuolization in the epithelium of proximal tubules and partially flattened distal tubule epithelium.

12074

International Journal of Nanomedicine 2024:19

3. Application of MPDAFe@DOX@Mem NPs for target CT-PTT, showed significant changes in oxidative stress parameters, manifested by an increase of kidney GSH, TBARS, CAT, and a decrease of SOD levels relative to the control group without treatment. Moreover, a higher CAT activity in the liver was also observed.

4. MPDAFe@DOX@Mem NPs with PTT increased kidney CAT activity and reduced liver TEAC levels compared to mice treated without laser irradiation, suggesting that combining PTT with these particles may intensify oxidative stress.

5. Higher TBARS levels were found in the kidneys of animals treated with MPDAFe@DOX@Mem NPs in CT-PTT, compared to the control and MPDAFe@Mem NPs groups, indicating increased lipid peroxidation.

6. Among animals from groups treated with MPDAFe@DOX@Mem NPs in combination with PTT, a TP concentration was significantly higher, than among animals of the groups treated just with MPDAFe@Mem NPs or TPP only.

7. In the kidneys of groups subjected to DOX therapies in combination with PDA nanoparticles, the concentration of glutathione was higher than in those without PDA, suggesting a nephroprotective effect. While TTP reduced this effect slightly, the levels remained significantly higher than the control.

8. Significantly fewer changes indicative of increased oxidative stress were noted in the livers of mice treated with MPDAFe@DOX@Mem NPs in combination with CT-PTT than in the kidneys, suggesting that this therapy may be more toxic to the kidneys.

Abbreviations

BW, body weight; CAT, catalase; CDBN, 1-chloro-2,4-dinitrobenzene; CT-PTT, chemo- and photothermal therapy; DOX, doxorubicin; DTNB, 5,5′-dithiobis(2-nitrobenzoic acid); GPX4, glutathione peroxidase; GSH, reduced glutathione; GST, glutathione S-transferase; HNE, 4-hydroxynonenal; H_2O_2, hydrogen peroxide; LOO•, peroxyl radicals; MDA, malondialdehyde; MPDAFe NPs, mesoporous polydopamine nanoparticles modified with iron; MPDAFe@DOX@Mem NPs, mesoporous polydopamine nanoparticles modified with iron coated with the cancer cell membrane and loaded with doxorubicin; MPDAFe@Mem NPs, nanoparticles modified with iron and coated with cancer cell membrane; NO, nitric oxide; NOS, nitric oxide synthase; O_2, molecular oxygen; ONOO-, peroxynitrite; PBS, phosphate-buffered saline solution; PDA, polydopamine; PDA NPs, polydopamine nanoparticles; PDT, photodynamic therapy; PTT, photothermal therapy; ROS, reactive oxygen species; RSNO, S-nitrosothiols; SDT, sonodynamic therapy; SOD, superoxide dismutase; TBARS, thiobarbituric acid reactive substances; TEAC, trolox equivalent antioxidant capacity; TMB, 1,3,5-trimethylbenzene; TP, total protein; UV, ultraviolet.

Acknowledgment

Disclosure

The authors report no conflicts of interest in this work.

References

1. Lee H, Dellatore SM, Miller WM, Messersmith PB. Mussel-inspired surface chemistry for multifunctional coatings. *Science*. 2007;318(5849):426–430. doi:10.1126/science.1147241

2. Hauser D, Septiadi D, Turner J, Petri-Fink A, Rothen-Rutishauser B. From bioinspired glue to medicine: polydopamine as a biomedical material. *Materials*. 2020;13(7):1730. doi:10.3390/ma13071730

3. Mrówczyński R. Polydopamine-based multifunctional (Nano)materials for cancer therapy. *ACS Appl Mater Interfaces*. 2018;10(9):7541–7561. doi:10.1021/acsami.7b08392

4. Ryu JH, Messersmith PB, Lee H. Polydopamine surface chemistry: a decade of discovery. *ACS Appl Mater Interfaces*. 2018;10(9):7523–7540. doi:10.1021/acsami.7b19865

5. Qu K, Wang Y, Vasileff A, Jiao Y, Chen H, Zheng Y. Polydopamine-inspired nanomaterials for energy conversion and storage. *J Mater Chem A*. 2018;6(44):21827–21846. doi:10.1039/C8TA05245J

6. Jin A, Wang Y, Lin K, Jiang L. Nanoparticles modified by polydopamine: working as "drug" carriers. *Bioact Mater*. 2020;5(3):522–541. doi:10.1016/j.bioactmat.2020.04.003

7. Chen R, Lin B, Luo R. Recent progress in polydopamine-based composites for the adsorption and degradation of industrial wastewater treatment. *Heliyon*. 2022;8(12):e12105. doi:10.1016/j.heliyon.2022.e12105

8. Im KM, Kim TW, Jeon JR. Metal-chelation-assisted deposition of polydopamine on human hair: a ready-to-use eumelanin-based hair dyeing methodology. *ACS Biomater Sci Eng*. 2017;3(4):628–636. doi:10.1021/acsbiomaterials.7b00031

9. Mrówczyński R, Bunge A, Liebscher J. Polydopamine–an organocatalyst rather than an innocent polymer. *Chemistry*. 2014;20(28):8647–8653. doi:10.1002/chem.201402532

10. Mrówczyński R, Markiewicz R, Liebscher J. Chemistry of polydopamine analogues. *Poly Int*. 2016; 2016:65. doi:10.1002/pi.5193

11. Chang C, Liu H, Li X, et al. Combined ROS responsive polydopamine-coated berberine nanoparticles effective against ulcerative colitis in mouse model. *Int J Nanomed*. 2024;19:1205–1224. doi:10.2147/IJN.S442761

12. Cui J, Yan Y, Such GK, et al. Immobilization and intracellular delivery of an anticancer drug using mussel-inspired polydopamine capsules. *Biomacromolecules*. 2012;13(8):2225–2228. doi:10.1021/bm300835r

13. Dobrzynska M, Napierala M, Florek E. Flavonoid nanoparticles: a promising approach for cancer therapy. *Biomolecules*. 2020;10(9):1268. doi:10.3390/biom10091268

14. Huang J, Guo L, Huang X, et al. Multimodal imaging-guided synergistic photodynamic therapy using carbonized Zn/Co Metal-organic framework loaded with cytotoxin against liver cancer. *Int J Nanomed*. 2024;19:4163–4180. doi:10.2147/IJN.S453275

15. Ambekar RS, Kandasubramanian B. A polydopamine-based platform for anti-cancer drug delivery. *Biomater Sci*. 2019;7(5):1776–1793. doi:10.1039/C8BM01642A

16. Zheng P, Ding B, Li G. Polydopamine-incorporated nanoformulations for biomedical applications. *Macromol Biosci*. 2020;20(12):e2000228. doi:10.1002/mabi.202000228

17. Acter S, Moreau M, Ivkov R, Viswanathan A, Ngwa W. Polydopamine nanomaterials for overcoming current challenges in cancer treatment. *Nanomaterials*. 2023;13(10):1656. doi:10.3390/nano13101656

18. Żebrowska K, Grabowska M, Coy E, Rolle K, Mrówczyński R, Grześkowiak BF. In vitro anticancer activity of melanin-like nanoparticles for multimodal therapy of glioblastoma. *Nanotechnol Rev*. 2024;13(1). doi:10.1515/ntrev-2023-0206

19. Menichetti A, Mordini D, Montalti M. Polydopamine nanosystems in drug delivery: effect of size, morphology, and surface charge. *Nanomaterials*. 2024;14(3):303. doi:10.3390/nano14030303

20. Liu H, Qu X, Tan H, et al. Role of polydopamine's redox-activity on its pro-oxidant, radical-scavenging, and antimicrobial activities. *Acta Biomater*. 2019;88:181–196. doi:10.1016/j.actbio.2019.02.032

21. Jędrzak A, Grześkowiak BF, Golba K, et al. Magnetite nanoparticles and spheres for chemo- and photothermal therapy of hepatocellular carcinoma in vitro. *Int J Nanomed*. 2020;15:7923–7936. doi:10.2147/IJN.S257142

22. Li M, Xuan Y, Zhang W, Zhang S, An J. Polydopamine-containing nano-systems for cancer multi-mode diagnoses and therapies: a review. *Int J Biol Macromol*. 2023;247:125826. doi:10.1016/j.ijbiomac.2023.125826

23. Li Z, Wang B, Zhang Z, et al. Radionuclide imaging-guided chemo-radioisotope synergistic therapy using a 131I-labeled polydopamine multi-functional nanocarrier. *Mol Ther*. 2018;26(5):1385–1393. doi:10.1016/j.ymthe.2018.02.019

24. Bigaj-Józefowska MJ, Grześkowiak BF. Polymeric nanoparticles wrapped in biological membranes for targeted anticancer treatment. *Eur Polym J*. 2022;176:111427. doi:10.1016/j.eurpolymj.2022.111427

25. Bigaj-Józefowska MJ, Coy E, Załęski K, et al. Biomimetic theranostic nanoparticles for effective anticancer therapy and MRI imaging. *J Photochem Photobiol B Biol*. 2023;249:112813. doi:10.1016/j.jphotobiol.2023.112813

26. Witkowska M, Mrówczyński R, Grześkowiak B, Miechowicz I, Florek E. Oxidative stress in xenograft mouse model exposed to dendrimers decorated polydopamine nanoparticles and targeted chemo- and photothermal therapy. *Int J Mol Sci*. 2023;24(23):16565. doi:10.3390/ijms242316565

27. Zhang B, Li Q, Xu Q, Li B, Dong H, Mou Y. Polydopamine modified ceria nanorods alleviate inflammation in colitis by scavenging ROS and regulating macrophage M2 polarization. *Int J Nanomed*. 2023;18:4601–4616. doi:10.2147/IJN.S416049

28. Da J, Li Y, Zhang K, et al. Functionalized Prussian blue nanozyme as dual-responsive drug therapeutic nanoplatform against maxillofacial infection via macrophage polarization. *Int J Nanomed*. 2022;17:5851–5868. doi:10.2147/IJN.S385899

29. Bao X, Zhao J, Sun J, Hu M, Yang X. Polydopamine nanoparticles as efficient scavengers for reactive oxygen species in periodontal disease. *ACS Nano*. 2018;12(9):8882–8892. doi:10.1021/acsnano.8b04022

30. Hu J, Yang L, Yang P, Jiang S, Liu X, Li Y. Polydopamine free radical scavengers. *Biomater Sci*. 2020;8(18):4940–4950. doi:10.1039/D0BM01070G

31. Florek E, Witkowska M, Szukalska M, et al. Oxidative stress in long-term exposure to multi-walled carbon nanotubes in male rats. *Antioxidants*. 2023;12(2):464. doi:10.3390/antiox12020464

32. Lowry OH, Rosebrough NJ, Farr AL, Randall RJ. Protein measurement with the folin phenol reagent. *J Biol Chem*. 1951;193(1):265–275. doi:10.1016/S0021-9258(19)52451-6

33. Konan MK, Koffi EN, Cisse I, Adima AA, Bekro YA. Phytochemical, nutritional and antioxidant capacity of five Ivorian edible leaves aqueous extracts. *J Appl Pharm Sci*. 2016;6(9):082–086. doi:10.7324/JAPS.2016.60912

34. Saville B. A scheme for the colorimetric determination of microgram amounts of thiols. *Analyst*. 1958;83(993):670–672. doi:10.1039/AN9588300670

35. Wang S, Circu ML, Zhou H, Figeys D, Aw TY, Feng J. Highly sensitive detection of s-nitrosylated proteins by capillary gel electrophoresis with laser induced fluorescence. *J Chromatogr A*. 2011;1218(38):6756–6762. doi:10.1016/j.chroma.2011.07.062

36. Bryan NS, Grisham MB. Methods to detect nitric oxide and its metabolites in biological samples. *Free Radic Biol Med*. 2007;43(5):645–657. doi:10.1016/j.freeradbiomed.2007.04.026

37. Rael LT, Thomas GW, Craun ML, Curtis CG, Bar-Or R, Bar-Or D. Lipid peroxidation and the thiobarbituric acid assay: standardization of the assay when using saturated and unsaturated fatty acids. *J Biochem Mol Biol*. 2004;37(6):749–752. doi:10.5483/bmbrep.2004.37.6.749

38. Ellman GL. Tissue sulfhydryl groups. *Arch Biochem Biophys*. 1959;82(1):70–77. doi:10.1016/0003-9861(59)90090-6

39. Bartosz G. *Druga Twarz Tlenu*. Wydawnictwo Naukowe PWN; 2006.

40. Valenti GE, Tasso B, Traverso N, Domenicotti C, Marengo B. Glutathione in cancer progression and chemoresistance: an update. *Redox Exp Med*. 2023;2023(1). doi:10.1530/REM-22-0023

41. Barrera G. Oxidative stress and lipid peroxidation products in cancer progression and therapy. *ISRN Oncol*. 2012;2012:137289. doi:10.5402/2012/137289

42. Holley AK, Miao L, St Clair DK, St Clair WH. Redox-modulated phenomena and radiation therapy: the central role of superoxide dismutases. *Antioxid Redox Signal*. 2014;20(10):1567–1589. doi:10.1089/ars.2012.5000

43. Kim EK, Jang M, Song MJ, Kim D, Kim Y, Jang HH. Redox-mediated mechanism of chemoresistance in cancer cells. *Antioxidants*. 2019;8 (10):471. doi:10.3390/antiox8100471

44. Domenicotti C, Marengo B. Paradox role of oxidative stress in cancer: state of the art. *Antioxidants*. 2022;11(5):1027. doi:10.3390/antiox11051027

45. Geng S, Feng Q, Wang C, et al. A versatile PDA(DOX) nanoplatform for chemo-photothermal synergistic therapy against breast cancer and attenuated doxorubicin-induced cardiotoxicity. *J Nanobiotechnology*. 2023;21(1):338. doi:10.1186/s12951-023-02072-1

46. Ju KY, Lee Y, Lee S, Park SB, Lee JK. Bioinspired polymerization of dopamine to generate melanin-like nanoparticles having an excellent free-radical-scavenging property. *Biomacromolecules*. 2011;12(3):625–632. doi:10.1021/bm101281b

47. Caldas M, Santos AC, Veiga F, Rebelo R, Reis RL, Correlo VM. Melanin nanoparticles as a promising tool for biomedical applications – a review. *Acta Biomater*. 2020;105:26–43. doi:10.1016/j.actbio.2020.01.044

48. Han J, Wang J, Shi H, et al. Ultra-small polydopamine nanomedicine-enabled antioxidation against senescence. *Mater Today Bio*. 2023;19:100544. doi:10.1016/j.mtbio.2023.100544

49. Mavridi-Printezi A, Menichetti A, Mordini D, Amorati R, Montalti M. Recent applications of melanin-like nanoparticles as antioxidant agents. *Antioxidants*. 2023;12(4):863. doi:10.3390/antiox12040863

50. Lou X, Hu Y, Zhang H, Liu J, Zhao Y. Polydopamine nanoparticles attenuate retina ganglion cell degeneration and restore visual function after optic nerve injury. *J Nanobiotechnology*. 2021;19:436. doi:10.1186/s12951-021-01199-3

51. Silva AV, Norinder U, Liiv E, Platzack B, Öberg M, Törnqvist E. Associations between clinical signs and pathological findings in toxicity testing. *ALTEX*. 2021;38(2):198–214. doi:10.14573/altex.2003311

52. Kuthati Y, Busa P, Tummala S, et al. Mesoporous polydopamine nanoparticles attenuate morphine tolerance in neuropathic pain rats by inhibition of oxidative stress and restoration of the endogenous antioxidant system. *Antioxidants*. 2021;10(2):195. doi:10.3390/antiox10020195

53. Han M, Li Y, Lu S, Yuan B, Cheng S, Cao C. Amyloid protein-biofunctionalized polydopamine nanoparticles demonstrate minimal plasma protein fouling and efficient photothermal therapy. *ACS Appl Mater Interfaces*. 2022;14(11):13743–13757. doi:10.1021/acsami.2c00716

54. Natarajan P, Tomich JM. Understanding the influence of experimental factors on bio-interactions of nanoparticles: towards improving correlation between in vitro and in vivo studies. *Arch Biochem Biophys*. 2020;694:108592. doi:10.1016/j.abb.2020.108592

55. Mahmoudi M, Landry MP, Moore A, Coreas R. The protein corona from nanomedicine to environmental science. *Nat Rev Mater*. 2023;1–17. doi:10.1038/s41578-023-00552-2

56. Zhang M, Zhang L, Chen Y, Li L, Su Z, Wang C. Precise synthesis of unique polydopamine/mesoporous calcium phosphate hollow Janus nanoparticles for imaging-guided chemo-photothermal synergistic therapy †Electronic supplementary information (ESI) available: FTIR spectroscopy, UV-vis absorption spectra, XRD, etc. *Chem Sci*. 2017;8(12):8067–8077. doi:10.1039/c7sc03521g

57. Li Y, Jiang C, Zhang D, et al. Targeted polydopamine nanoparticles enable photoacoustic imaging guided chemo-photothermal synergistic therapy of tumor. *Acta Biomater*. 2017;47:124–134. doi:10.1016/j.actbio.2016.10.010

58. Traverso N, Ricciarelli R, Nitti M, et al. Role of glutathione in cancer progression and chemoresistance. *Oxid Med Cell Longev*. 2013;2013:972913. doi:10.1155/2013/972913

59. Zou M, Hu X, Xu B, et al. Glutathione S-transferase isozyme alpha 1 is predominantly involved in the cisplatin resistance of common types of solid cancer. *Oncol Rep*. 2019;41(2):989–998. doi:10.3892/or.2018.6861

60. Marini HR, Facchini BA, Di Francia R, et al. Glutathione: lights and shadows in cancer patients. *Biomedicines*. 2023;11(8):2226. doi:10.3390/biomedicines11082226

61. Sato M, Kusumi R, Hamashima S, et al. The ferroptosis inducer erastin irreversibly inhibits system xc- and synergizes with cisplatin to increase cisplatin's cytotoxicity in cancer cells. *Sci Rep*. 2018;8(1):968. doi:10.1038/s41598-018-19213-4

62. Kennedy L, Sandhu JK, Harper ME, Cuperlovic-Culf M. Role of glutathione in cancer: from mechanisms to therapies. *Biomolecules*. 2020;10 (10):1429. doi:10.3390/biom10101429

63. Shen B-Y, Chen C, Xu Y-F. Is the combinational administration of doxorubicin and glutathione a reasonable proposal? *Acta Pharmacol Sin*. 2019;40(5):699–709. doi:10.1038/s41401-018-0158-8

64. Feng J, Gao JL, Zhang RY, Ren WX, Dong YB. Polydopamine-based multifunctional antitumor nanoagent for phototherapy and photodiagnosis by regulating redox balance. *ACS Appl Bio Mater*. 2020;3(12):8667–8675. doi:10.1021/acsabm.0c01057

65. Singh RR, Reindl KM. Glutathione S-transferases in cancer. *Antioxidants*. 2021;10(5):701. doi:10.3390/antiox10050701

66. Lv N, Huang C, Huang H, et al. Overexpression of glutathione S-transferases in human diseases: drug targets and therapeutic implications. *Antioxidants*. 2023;12(11):1970. doi:10.3390/antiox12111970

67. Beckett GJ, Hayes JD. Glutathione S-transferases: biomedical applications. *Adv Clin Chem*. 1993;30:281–380. doi:10.1016/s0065-2423(08)60198-5

68. Pérez de la Lastra JM, Juan CA, Plou FJ, Pérez-Lebeña E. The nitration of proteins, lipids and DNA by peroxynitrite derivatives-chemistry involved and biological relevance. *Stresses*. 2022;2(1):53–64. doi:10.3390/stresses2010005

69. Hess DT, Matsumoto A, Kim SO, Marshall HE, Stamler JS. Protein S-nitrosylation: purview and parameters. *Nat Rev Mol Cell Biol*. 2005;6 (2):150–166. doi:10.1038/nrm1569

70. Nakamura T, Lipton SA. Nitric oxide-dependent protein post-translational modifications impair mitochondrial function and metabolism to contribute to neurodegenerative diseases. *Antioxid Redox Signal*. 2020;32(12):817–833. doi:10.1089/ars.2019.7916

71. Canuto RA, Muzio G, Maggiora M, Biocca ME, Dianzani MU. Glutathione-*S*-transferase, alcohol dehydrogenase and aldehyde reductase activities during diethylnitrosamine-carcinogenesis in rat liver. *Cancer Lett*. 1993;68(2):177–183. doi:10.1016/0304-3835(93)90144-X

72. Lykkesfeldt J. Malondialdehyde as biomarker of oxidative damage to lipids caused by smoking. *Clin Chim Acta*. 2007;380(1–2):50–58. doi:10.1016/j.cca.2007.01.028

73. Mishima E, Conrad M. Nutritional and metabolic control of ferroptosis. *Annu Rev Nutr*. 2022;42:275–309. doi:10.1146/annurev-nutr-062320-114541

74. Zhang Y, Ren X, Wang Y, et al. Targeting ferroptosis by polydopamine nanoparticles protects heart against ischemia/reperfusion injury. *ACS Appl Mater Interfaces*. 2021;13(45):53671–53682. doi:10.1021/acsami.1c18061

75. Lei L, Yuan J, Yang Q, et al. Curcumin–polydopamine nanoparticles alleviate ferroptosis by iron chelation and inhibition of oxidative stress damage. *RSC Adv*. 2024;14(21):14934–14941. doi:10.1039/D4RA02336F

76. Yu H, Yan J, Li Z, Yang L, Ju F, Sun Y. Recent trends in emerging strategies for ferroptosis-based cancer therapy. *Nanoscale Adv*. 2023;5(5):1271–1290. doi:10.1039/D2NA00719C

77. Ding X, Wang Z, Yu Q, et al. Superoxide dismutase-like regulated Fe/Ppa@PDA/B for synergistically targeting ferroptosis/apoptosis to enhance anti-tumor efficacy. *Adv Healthc Mater*. 2023;12(29):e2301824. doi:10.1002/adhm.202301824

78. Hu H, Yang J, Zhong Y, et al. Polydopamine-Pd nanozymes as potent ROS scavengers in combination with near-infrared irradiation for osteoarthritis treatment. *iScience*. 2023;26(5):106605. doi:10.1016/j.isci.2023.106605

79. Doskey CM, Buranasudja V, Wagner BA, et al. Tumor cells have decreased ability to metabolize H2O2: implications for pharmacological ascorbate in cancer therapy. *Redox Biol*. 2016;10:274–284. doi:10.1016/j.redox.2016.10.010

80. Galasso M, Gambino S, Romanelli MG, Donadelli M, Scupoli MT. Browsing the oldest antioxidant enzyme: catalase and its multiple regulation in cancer. *Free Radic Biol Med*. 2021;172:264–272. doi:10.1016/j.freeradbiomed.2021.06.010

81. Perillo B, Di Donato M, Pezone A, et al. ROS in cancer therapy: the bright side of the moon. *Exp Mol Med*. 2020;52(2):192–203. doi:10.1038/s12276-020-0384-2

82. Bai J, Cederbaum AI. Catalase protects HepG2 cells from apoptosis induced by DNA-damaging Agents by accelerating the degradation of p53. *J Biol Chem*. 2003;278(7):4660–4667. doi:10.1074/jbc.M206273200

83. Small DM, Coombes JS, Bennett N, Johnson DW, Gobe GC. Oxidative stress, anti-oxidant therapies and chronic kidney disease. *Nephrology*. 2012;17(4):311–321. doi:10.1111/j.1440-1797.2012.01572.x

84. Shi J, Yang Y, Yin N, et al. Engineering CXCL12 biomimetic decoy-integrated versatile immunosuppressive nanoparticle for ischemic stroke therapy with management of overactivated brain immune microenvironment. *Small Methods*. 2022;6(1):e2101158. doi:10.1002/smtd.202101158

85. O'Connor NA, Syed A, Wong M, et al. Polydopamine antioxidant hydrogels for wound healing applications. *Gels*. 2020;6(4):39. doi:10.3390/gels6040039

86. Carmignani A, Battaglini M, Sinibaldi E, et al. In vitro and ex vivo investigation of the effects of polydopamine nanoparticle size on their antioxidant and photothermal properties: implications for biomedical applications. *ACS Appl Nano Mater*. 2022;5(1):1702–1713. doi:10.1021/acsanm.1c04536